Arabian Journal of Geosciences (2021) 14: 212
https://doi.org/10.1007/s12517-020-06437-w

ORIGINAL PAPER

Zircon U–Pb ages and petrogenesis of the middle Eocene Aliabad Daman pluton, Northeast Iran: implications for magmatic activity along the Doruneh fault zone

Hossein Shahbazi[1] · Ali Asghar Sepahi[1] · Mohammad Amin Shakouri[1]

Received: 8 September 2020 / Accepted: 30 December 2020 / Published online: 31 January 2021

Abstract

The Aliabad Daman pluton is exposed along the Doruneh fault zone of the southern edge of the Sabzevar zone, northeast Iran. This intrusive body consists of alkali feldspar granite, syenogranite, and monzogranite. U–Pb age dating results demonstrate that the magmas crystallized 45–40 Ma ago in the middle Eocene (Lutetian to Bartonian). Whole-rock samples show SiO_2 ranging between 75.4 and 77.0 wt.%, variable fractionation between light and heavy rare earth elements (REE) (La_N/Yb_N = 11–22) with negative Eu anomalies Eu/Eu* (0.1–0.4), depletion of heavy REE, enrichment of large ion lithophile elements (LILE), and plot in the metaluminous to peraluminous, and high-K calc-alkaline fields. The major and trace element characteristics of the Aliabad Daman pluton bear the imprints of the partial melting process. The presence of inherited zircon and the combination of the new results with previous studies suggest that the magma of the Aliabad Daman pluton was derived from a continental crustal source and an enriched mantle source. Tectonic activities such as the shortening and the thickening of the continental crust, delamination of the lower crust and the lithospheric mantle, heating by upwelling asthenosphere, and tectonic activities along the Doruneh fault zone on the southern edge of the Sabzevar zone as well as the extensional collapse of the crust played important roles in the generation and emplacement of the Aliabad Daman pluton.

Keywords Aliabad Daman pluton · Zircon U-Pb age dating · Extensional collapse · Doruneh fault zone · Sabzevar zone

Introduction

Extensive middle Eocene to recent alkaline and calc-alkaline magmatic rocks, mainly volcanic and unrelated to subduction processes, are present in Iran between Arabia and Eurasia. The origin of these rocks is related to shortening and thickening processes of the continental crust. Major fault systems such as the Doruneh fault zone have played an important role in the generation and emplacement of the magmas (Berberian and King 1981). Magmatism lasted from the middle Eocene (*c.* 46 Ma) to the Late Oligocene (*c.* 25 Ma). In the Lut–Sistan region, this magmatism can best be explained by lithospheric removal and asthenospheric upwelling associated with the extensional collapse of the east Iranian ranges (Pang et al. 2013).

Post-kinematic intrusions of Eocene age (47–44 Ma) occur in the western part of the Saghand area (Fig. 1a). Their formation is related to the convergence between Arabian and Eurasian plates and the Cenozoic closure of the Tethys oceanic tract(s) (Ramezani and Tucker 2003). In the Khaf-Kashmar-Bardaskan belt (Fig. 1b), subduction of the Neotethys was followed by collision and post-collision suturing and magmatism, during the Early Tertiary. Significant Eocene plutonism is related to an extensional setting triggered by heating and melt generation in a subduction-modified mantle by upwelling of asthenospheric mantle even far from the Neotethyan subduction zone (Alizadeh et al. 2017).

A magmatic flare-up occurred during the Late Paleocene-Eocene in the Urumieh-Dokhtar belt and the Alborz Mountains, central Iran. This flare-up was accompanied by normal faulting (Verdel et al. 2011). Whole rock geochemical and geochronological data suggest that this flare-up was extension related and the resulting melts show typical

Responsible Editor: Domenico M. Doronzo

✉ Hossein Shahbazi
shahbazi.h@gmail.com; shahbazi@basu.ac.ir

[1] Department of Geology, Faculty of Sciences, Bu-Ali Sina University, Hamedan, Iran

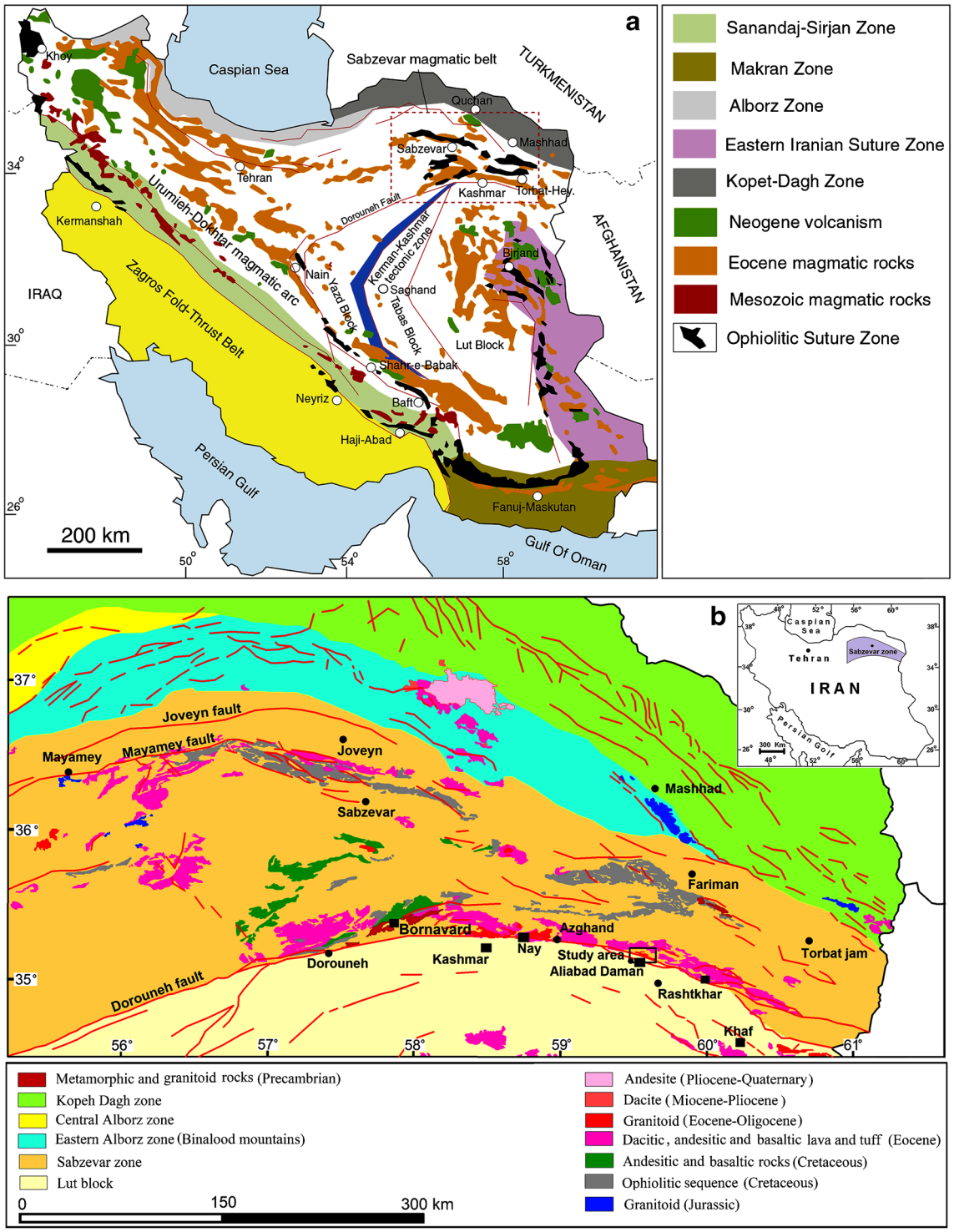

Fig. 1 (**a**) Simplified geological map of Iran showing the distribution of Eocene magmatic rocks (modified after Shafaii Moghadam et al. 2015), (**b**) geological and tectonic zones, and simplification of igneous rocks and location of the Aliabad Daman pluton in the Sabzevar Ophiolitic Suture zone (NE Iran). Tectonic zones and location of magmatic rocks redrawn from the geological map of Iran 1:1000000, Geological Survey of Iran (Sahandi and Soheili, 2014)

characteristics of continental arc magmas, whereas the Oligocene basalts, which were erupted after the flare-up, are more consistent with derivation from the asthenospheric mantle (Verdel et al. 2011).

The Doruneh fault (Fig. 1b) is a major transcurrent fault, extending *c.* 900 km from western Afghanistan to West-Central Iran. It is also a key structure in the Arabia–Eurasia collisional zone, bounding the northern margin of the central

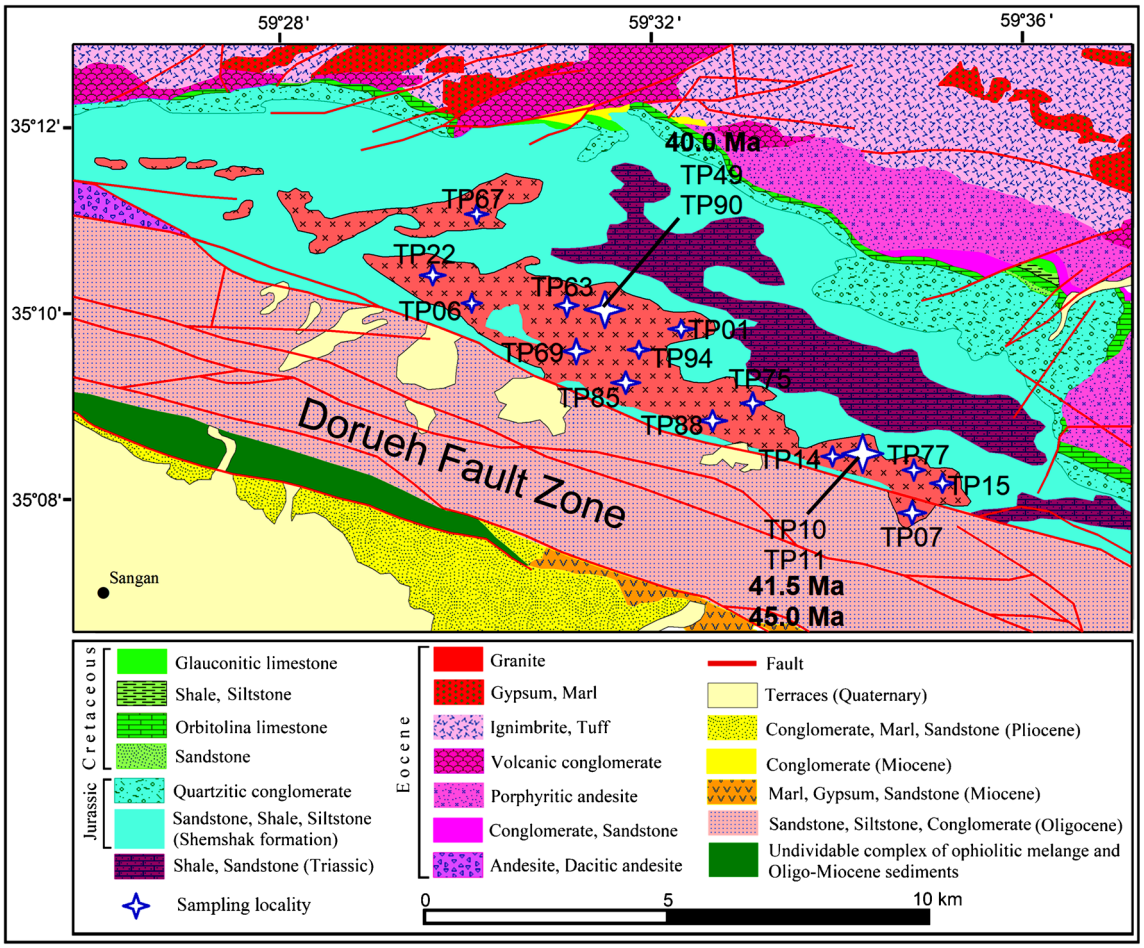

Fig. 2 Geological map of the Aliabad Daman granite area,Sabzevar zone, NE- Iran and sampling locality, redrawn from regional geological map of Dolatabad and Torbat-e-Heydarieh 1:100000, Geological Survey of Iran (Kholghi Khosraghi 1996a, b)

Iranian microcontinent (CIM) block. Javadi et al. (2013) report an Eocene (*c.* 56 Ma) initiation age and a slip rate of about 5.2–5.5 mm year^{-1} of the fault, which accompanied the 35° anticlockwise rotation of the CIM. The Doruneh fault operated as a major zone of residual stress transfer and accommodation in Central Iran. The tectonic evolution of the fault was modulated by convergent plate boundary dynamics (Tadayon et al. 2017). By combining the structural, stratigraphic, and thermochronological dataset, a tectono-stratigraphic evolutionary model for the Doruneh fault has been proposed (Tadayon et al. 2018). In this model, the Sabzevar back-arc oceanic domain started to form during the upper Cretaceous, and the rotation of the CIM along the Doruneh fault zone is placed within the Paleocene-Eocene epoch (60–40 Ma).

The Sabzevar structural zone (Fig. 1) hosts numerous post-ophiolite middle Eocene volcanic rocks. Some of these rocks emplaced along major faults, such as the Sabzevar, Mayamey and Doruneh faults at the southern Sabzevar zone (Fig. 1b). Middle Eocene igneous rocks in the Sabzevar zone can be divided into two main groups, (1) adakitic rocks with ages of *c.* 47 Ma (Alaminia et al. 2013; Rossetti et al. 2014; Jamshidi et al. 2015b; Shafaii Moghadam et al., 2016; Jamshidi et al. 2018), and (2) igneous rocks without adakitic affinities and ages of *c.* 40 Ma (Shafaii Moghadam et al. 2015; Alizadeh et al. 2017; Almasi et al. 2019; this study).

The Aliabad-Daman pluton (Fig. 2) is located along the Doruneh fault zone at the southern edge of the Sabzevar structural zone, 25 km northwest of Rashtkhar and 10 km from Aliabad-Daman, northeast Iran. So far, no geochronological studies have yet been performed on this pluton. In the geological map of Dolatabad and Torbat-e-Heydarieh, this pluton has been mapped as a post middle Jurassic granite (Kholghi Khosraghi 1996a, b). Here, we present petrographic, whole rock geochemical, and zircon U-Pb ages for the Aliabad-Daman pluton. On the basis of the new results in combination with previous studies, an explanation of how various tectonic processes controlled the injection of the granitic melts in the Eocene is given.

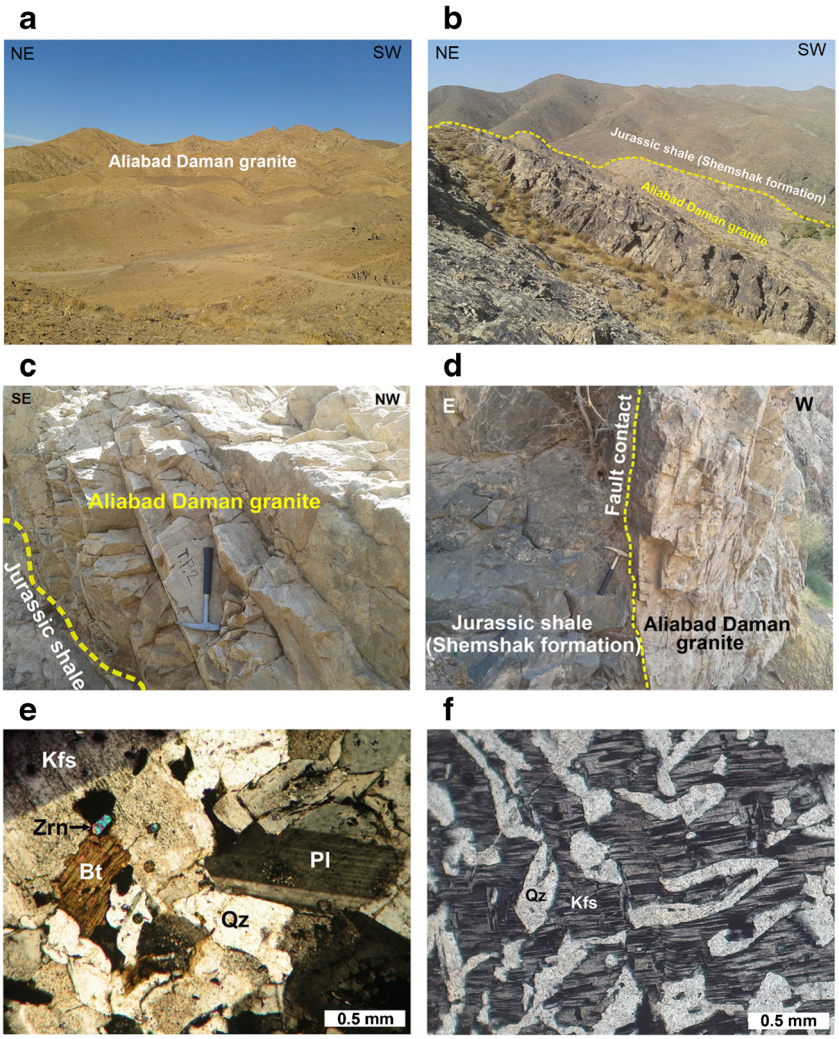

Fig. 3 **a** Field photographic view of the Aliabad Daman granite. **b**, **c**, **d** Field photograph from contact between Jurassic shale of the Shemshak Formation and the Aliabad Daman granite. **e** Polarized microscopic image showing granular texture, quartz, K-feldspar, plagioclase, Biotite and zircon in the Aliabad Daman granite. **f** Polarized microscopic image showing granophyric texture in the Aliabad Daman igneous body. Abbreviation symbols (Whitney and Evans 2010); Pl = plagioclase, Kfs = K-feldspar, Qz = quartz, Bt = biotite, Zrn = zircon

Geological setting

The Sabzevar zone is located at the northern margin of the central Iranian microcontinent (Takin 1972), northeast Iran. This zone extends east–west and is separated to the north by the Maymey and Joveyn faults from the Alborz-Binalood and Kopet Dagh mountains of the Turan plate, and to the south by the Doruneh fault from the Lut block (Fig. 1).

The occurrence of early Cretaceous deep marine sediments, ophiolites and mélange complexes led to a model that three inner Mesozoic Oceans surrounded the central Iranian microcontinent (CIM) block. (1) Sabzevar Ocean, that was located in the north of the CIM, and separated the CIM from the Turan and Kopeh Dagh plates. (2) Sistan Ocean, that was located in the east of the CIM, and separated the CIM from the Farah and Helmand blocks in Afghanistan. (3) Baft-Nain Ocean that was located in the west–southwest of the CIM, and separated the CIM from the Sanandaj–Sirjan zone and Afro-Arabian plate (e.g., Sengör et al. 1988; Sengör 1990; McCall 1997; Shojaat et al. 2003; Baroz et al. 1984; Arvin and Robinson 1994; Agard et al. 2011). Some authors assume that the Baft-Nain Ocean was connected to the Sistan basin (Saccani et al. 2010; Agard et al. 2011; Bonnet et al. 2020).

The basement of the Sabzevar zone is composed of Late Neoproterozoic to Early Cambrian (Cadomian) magmatic rocks. Outcrops of these rocks can be found in the Taknar-Bornaward and Fariman regions (Fig. 1b). Based on the Kashmar geological map, the Cadomian basement of the Sabzevar zone in Doruneh and Kashmar regions consists of brecciaed metarhyolite (Taheri and Shamanian 2001). The Arghash dioritic pluton with a U–Pb zircon age of 554 ± 6 Ma is reported from the Sabzevar zone (Alaminia et al. 2013). Based on inherited zircon record, it was suggested that 10–20 vol.% of the middle Eocene Kashmar granitoid (Fig. 1) has been formed from the Cadomian lower crust (Shafaii Moghadam et al. 2015). The age of the Taknar and Bornaward granitoid complex (Fig. 1) is Late-Neoproterozoic (570–530 Ma) (Monazzami Bagherzadeh et al. 2015; Shafaii Moghadam et al. 2017). Detail geochronological data show that the plutonic rocks of the Taknar zone

Table 1 U-Pb isotopic data for zircon crystal determined by LA-ICP-MS in plutonic rocks of the Aliabad Daman granite, Sabzevar zone, NE Iran

TP4990-04 (Syenogranite)										
Spot	Th/U	207Pb/235 U	Error (±2σ)	206Pb/238 U	Error (±2σ)	rho	235 U-207Pb (Ma)	Error (±2σ)	238 U-206Pb (Ma)	Error (±2σ)
TP4990-01	0.72	0.04478	0.00799	0.006194	0.000276	0.05243	44.5	7.9	39.8	1.8
TP4990-02	0.53	0.04215	0.00703	0.006102	0.000254	0.05010	41.9	7.0	39.2	1.6
TP4990-03	0.96	0.04055	0.00339	0.006413	0.000170	0.04586	40.4	3.4	41.2	1.1
TP4990-04	0.85	0.04577	0.00530	0.006501	0.000210	0.05106	45.4	5.3	41.8	1.3
TP4990-05*	0.41	0.13525	0.01399	0.007554	0.000293	0.12985	128.8	13.3	48.5	1.9
TP4990-06	0.56	0.03735	0.00483	0.006160	0.000205	0.04397	37.2	4.8	39.6	1.3
TP4990-07	0.77	0.03787	0.00437	0.006151	0.000192	0.04466	37.7	4.4	39.5	1.2
TP4990-08	0.61	0.05327	0.00610	0.006052	0.000207	0.06384	52.7	6.0	38.9	1.3
TP4990-09	0.32	0.03942	0.00527	0.006022	0.000194	0.04749	39.3	5.2	38.7	1.2
TP4990-10	0.53	0.03344	0.00543	0.006245	0.000213	0.03884	33.4	5.4	40.1	1.4
TP4990-11*	0.60	0.57719	0.03900	0.011511	0.000399	0.36366	462.6	31.3	73.8	2.6
TP4990-12	0.64	0.04061	0.00570	0.006052	0.000203	0.04867	40.4	5.7	38.9	1.3
TP4990-13	0.64	0.05076	0.00482	0.006064	0.000171	0.06071	50.3	4.8	39.0	1.1
TP4990-14	0.65	0.06610	0.00781	0.006258	0.000216	0.07661	65.0	7.7	40.2	1.4
TP4990-15	0.64	0.04633	0.00388	0.006236	0.000160	0.05388	46.0	3.8	40.1	1.0
TP4990-16	0.25	0.03498	0.00444	0.006022	0.000182	0.04213	34.9	4.4	38.7	1.2
TP4990-17	0.83	0.04213	0.00478	0.006417	0.000169	0.04762	41.9	4.8	41.2	1.1
TP4990-18	0.97	0.04535	0.00413	0.006086	0.000142	0.05405	45.0	4.1	39.1	0.9
TP4990-19	0.63	0.03887	0.00612	0.006271	0.000205	0.04496	38.7	6.1	40.3	1.3
TP4990-20	0.55	0.03793	0.00538	0.006351	0.000190	0.04331	37.8	5.4	40.8	1.2
TP4990-21	0.91	0.04577	0.00774	0.006160	0.000227	0.05389	45.4	7.7	39.6	1.5
TP4990-22	0.74	0.03950	0.00489	0.006361	0.000175	0.04503	39.3	4.9	40.9	1.1
TP4990-23	0.64	0.05132	0.00655	0.006541	0.000199	0.05690	50.8	6.5	42.0	1.3
TP4990-24	1.33	0.03847	0.00474	0.006128	0.000168	0.04553	38.3	4.7	39.4	1.1
TP4990-25	0.85	0.03492	0.00426	0.006093	0.000206	0.04156	34.8	4.3	39.2	1.3
TP4990-26	0.80	0.03954	0.00431	0.005964	0.000197	0.04808	39.4	4.3	38.3	1.3
TP4990-27	0.89	0.04860	0.00636	0.006417	0.000238	0.05493	48.2	6.3	41.2	1.5
TP4990-28	0.73	0.04722	0.00611	0.006621	0.000241	0.05173	46.9	6.1	42.5	1.5
TP4990-29	0.73	0.03845	0.00561	0.006130	0.000230	0.04549	38.3	5.6	39.4	1.5
TP4990-30	0.63	0.03983	0.00420	0.006225	0.000202	0.04640	39.7	4.2	40.0	1.3
TP4990-31	0.71	0.04395	0.00496	0.006436	0.000217	0.04953	43.7	4.9	41.4	1.4
TP4990-32	0.54	0.05249	0.00658	0.006188	0.000231	0.06152	51.9	6.5	39.8	1.5
TP4990-33	0.62	0.04874	0.00594	0.006233	0.000184	0.05671	48.3	5.9	40.1	1.2
TP4990-34*	2.21	0.29087	0.02120	0.008094	0.000259	0.26062	259.2	18.9	52.0	1.7
TP4990-35	0.72	0.05122	0.00631	0.006321	0.000191	0.05876	50.7	6.2	40.6	1.2
TP4990-36	0.68	0.06378	0.00633	0.006258	0.000173	0.07391	62.8	6.2	40.2	1.1
TP4990-37	0.70	0.06967	0.00596	0.006190	0.000158	0.08163	68.4	5.8	39.8	1.0
TP4990-38	0.62	0.03844	0.00638	0.006113	0.000213	0.04561	38.3	6.4	39.3	1.4
TP4990-39	0.80	0.05029	0.00664	0.006400	0.000203	0.05699	49.8	6.6	41.1	1.3
TP4990-40	0.75	0.04285	0.00533	0.006172	0.000178	0.05036	42.6	5.3	39.7	1.1
TP-1011 (Alkali feldspar granite)										
Spot	Th/U	207Pb/235 U	Error (±2σ)	206Pb/238 U	Error (±2σ)	rho	235 U-207Pb (Ma)	Error (±2σ)	238 U-206Pb (Ma)	Error (±2σ)
TP-1011-01	0.64	0.0529	0.0059	0.00726	0.00023	0.285	52.3	5.8	46.6	1.5
TP-1011-02	0.78	0.0431	0.0037	0.00659	0.00018	0.319	42.8	3.6	42.3	1.1
TP-1011-03	0.88	0.0462	0.0055	0.00663	0.00022	0.274	45.8	5.4	42.6	1.4
TP-1011-04*	2.86	11.1020	1.4348	0.09414	0.00704	0.579	2531.6	327.2	580.0	43.4
TP-1011-05*	1.12	0.3813	0.0171	0.00663	0.00018	0.613	328.0	14.7	42.6	1.2

Table 1 (continued)

TP-1011-06	0.63	0.0585	0.0075	0.00718	0.00026	0.278	57.8	7.4	46.1	1.6
TP-1011-07*	2.32	12.8916	1.6398	0.10947	0.00807	0.580	2671.7	339.8	669.7	49.4
TP-1011-08*	2.29	1802.3966	958.5512	15.26093	6.19744	0.754	7612.5	4048.5	17,977.5	7300.6
TP-1011-09	0.85	0.0394	0.0046	0.00646	0.00016	0.214	39.2	4.6	41.5	1.0
TP-1011-10	0.75	0.0419	0.0050	0.00676	0.00017	0.215	41.7	5.0	43.4	1.1
TP-1011-11	0.58	0.0513	0.0055	0.00629	0.00016	0.243	50.8	5.4	40.5	1.1
TP-1011-12	0.85	0.0417	0.0038	0.00640	0.00013	0.228	41.5	3.8	41.1	0.9
TP-1011-13	0.56	0.0411	0.0051	0.00621	0.00017	0.220	40.9	5.1	39.9	1.1
TP-1011-14	0.63	0.0758	0.0073	0.00678	0.00018	0.278	74.2	7.2	43.6	1.2
TP-1011-15	0.66	0.0468	0.0047	0.00691	0.00016	0.228	46.5	4.7	44.4	1.0
TP-1011-16	0.48	0.0717	0.0087	0.00715	0.00023	0.261	70.3	8.6	45.9	1.5
TP-1011-17	0.65	0.0407	0.0063	0.00661	0.00029	0.280	40.6	6.3	42.5	1.8
TP-1011-18	1.38	0.0817	0.0061	0.00696	0.00025	0.482	79.8	6.0	44.7	1.6
TP-1011-19	0.21	0.0587	0.0048	0.00648	0.00023	0.442	57.9	4.7	41.6	1.5
TP-1011-20	0.53	0.0601	0.0080	0.00686	0.00030	0.327	59.3	7.9	44.1	1.9
TP-1011-21*	2.88	11.1533	1.1303	0.10257	0.00628	0.604	2535.9	257.0	629.5	38.6
TP-1011-22	0.79	0.0769	0.0047	0.00691	0.00024	0.560	75.2	4.6	44.4	1.5
TP-1011-23	1.02	0.0970	0.0107	0.00737	0.00032	0.390	94.0	10.3	47.3	2.0
TP-1011-24	0.90	0.1147	0.0129	0.00698	0.00032	0.404	110.2	12.4	44.8	2.0

*Not use in Concordia diagram

in the Kaboodan area mainly formed during the late Neoproterozoic (550–530 Ma, (Mazhari et al. 2019).

Upper Cretaceous igneous rocks in the Sabzevar zone can be divided into two main groups, (i) ophiolitic igneous rocks and (ii) the non-ophiolitic, subduction-related igneous rocks. The ophiolitic igneous rocks are NW-SE orientated and are mostly found along faults (Fig. 1b). The Sabzevar ophiolite originated from a tholeiitic magma source in an intra-oceanic island arc/supra-subduction zone setting (Rahmani et al. 2017). The non-ophiolitic, subduction-related igneous rocks in the Sabzevar zone are exposed as both intrusive and extrusive rocks. These rocks crop out mostly southwest and south of Sabzevar (Fig. 1b). The non-ophiolitic rocks formed during upper Cretaceous time between *c.* 101–75 Ma. In the Arghash region, I-type granitoids with ages of *c.* 93 Ma originated in an island-arc or back-arc basin setting (Alaminia et al. 2013). A series of shallow mafic to felsic rocks that are intrusive and extrusive with ages of 101–75 Ma have been formed in a supra-subduction system (Kazemi et al. 2019). In the Kaboodan region, there are extrusive and intrusive rocks with ages between 99 and 75 Ma (Mazhari et al. 2019).

The Sabzevar zone hosts abundant early to middle Eocene (57–45 Ma) adakitic intrusions, mainly of extrusive nature (Fig. 1b). This magmatism occurred during the collision between the central Iranian microcontinent (CIM) block and the Turan block between *c.* 57 and 45 Ma. A suite of felsic magmatic rocks with zircon U-Pb ages of *c.* 58 Ma crop out in the Soltanabad area of the Sabzevar zone (Rossetti et al. 2014). Adakitic igneous bodies of andesite, dacite and fine-grained granite with ages of *c.* 55 Ma occur in the Arghash region (Alaminia et al. 2013). Adakitic intermediate to felsic mainly extrusive and minor intrusive rocks with zircon U–Pb and mica Ar–Ar ages of 47–45 Ma are found northwest of Sabzevar (Shafaii Moghadam et al. 2014; Shafaii Moghadama et al. 2016). Numerous middle Eocene (*c.* 45 Ma) extrusive intermediate to felsic rocks intruded into the Sabzevar ophiolitic belt northwest of Sabzevar (Jamshidi et al. 2018). Post-ophiolitic high-silica adakitic rocks with emplacement ages of *c.* 48 Ma and dacite/rhyolite composition outcrop in the ophiolitic complex of the Sabzevar zone (Jamshidi et al. 2015b).

In addition, several intrusive rocks without adakitic affinities and of middle Eocene and Bartonian age (*c.* 40 Ma) intruded into the Sabzevar zone along the major Doruneh fault zone. So far, some researchers (Shafaii Moghadam et al. 2015; Alizadeh et al. 2017; Almasi et al. 2019) have studied three similar plutons along the Doruneh fault zone from the Sabzevar zone and the Lut block. The Aliabad-Daman pluton occurs along the Doruneh fault zone, 10 km north of Aliabad Daman, 12 km northeast of Sangan, 25 km northwest of Rashtkhar and the southern edge of the Sabzevar structural zone (Fig. 2). This pluton consists of alkali feldspar granite, syenogranite, and monzogranite. The Aliabad-Daman pluton intruded into the Shemshak Formation containing Jurassic sandstone, siltstone, shale, and claystone, and the Nayband Formation containing Triassic sandstone and shale. The concentration of Eocene magmatic rocks along the Doruneh fault zone shows that this major fault zone, with a length of 900 km, exerted an important role in the emplacement of the Eocene magmatism on the southern edge of the Sabzevar structural zone (Fig. 1).

Field relations and petrography

Rocks of the Aliabad Daman pluton (Figs. 1, 2) have a massive structure, a leucocratic appearance and a color index of 5–

Fig. 4 **a** Cathodoluminescence (CL) images of the zircon grains of sample TP4940 (Syenogranite). **b** Cathodoluminescence (CL) images of the zircon grains of the sample TP1011 (Alkali feldspar granite) with positions of the ablation

15. (Fig. 3a–d). The pluton has fault-bounded contacts with Jurassic shales of the Shemshak Formation (Fig. 3 e). The pluton consists of syenogranites, alkali feldspar granites, and monzogranites with mainly granular (Fig. 3f) and minor granophyric textures (Fig. 3d). Syenogranites form the main volume (~50%) of the pluton and are composed of 30–50 vol.% quartz, 20–40 vol.% alkali feldspar, 5–15 vol.% plagioclase and accessory minerals of biotite, titanite, apatite and zircon. Alkali feldspar granites make up about 30% of the volume of the Aliabad Daman pluton. Mineral constituents are alkali feldspar 40–50 vol.%, quartz 20–30 vol.%, plagioclase 5–10 vol.%, and apatite, titanite, and zircon occur as accessory mineral phases. Monzogranites make up a smaller volume of the pluton with a mineral assemblage of 25–30 vol.% quartz, 25–30 vol.% plagioclase, 20–30 vol.% alkali feldspar, 5–10 vol.% biotite, and accessory minerals including titanite, apatite, and zircon.

Analytical methods

Fifty-five samples from the Aliabad Daman granite with the least signs of alteration were selected for analyses. Thin sections were prepared from all samples and studied under an optical polarized microscope (Zeiss-Axioskop 40 POL) at the Department of Geology, Bu-Ali Sina

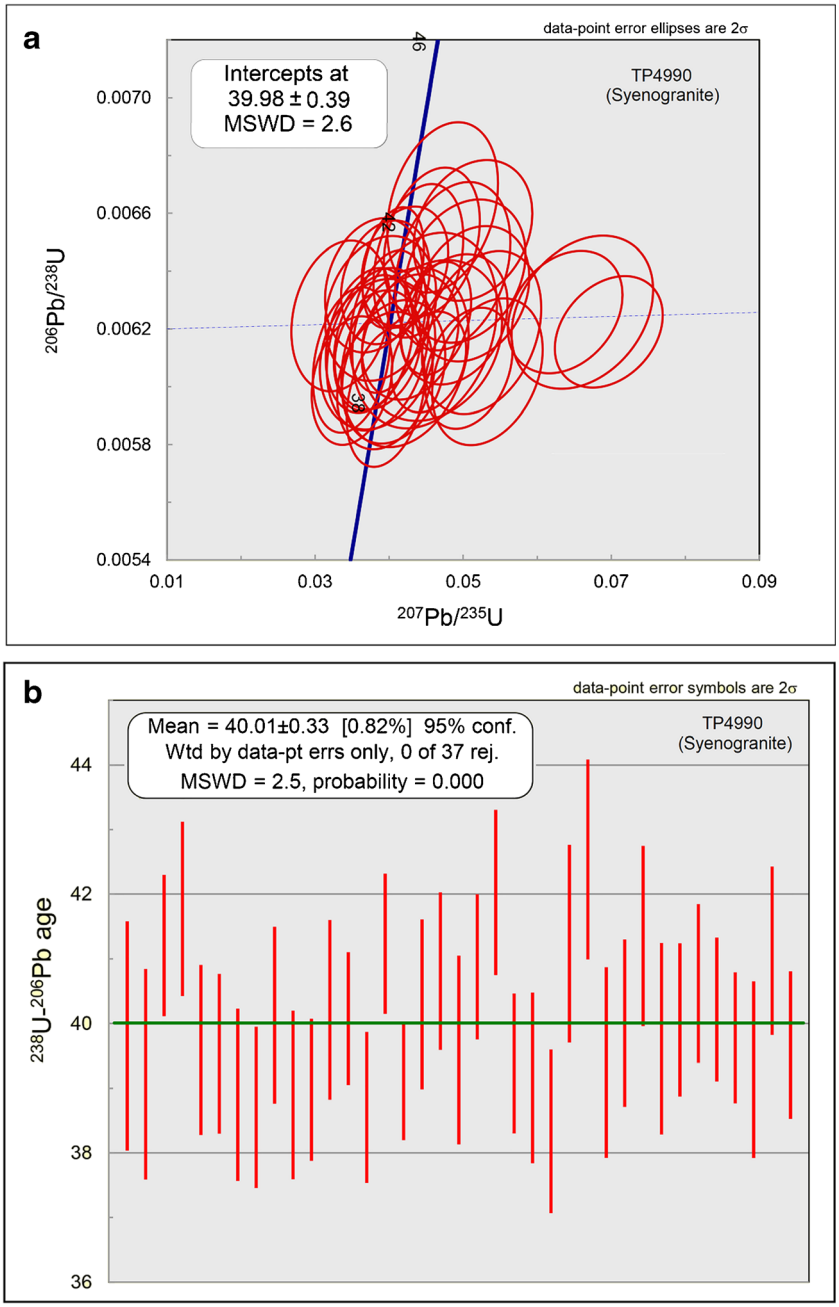

Fig. 5 Zircon U–Pb Concordia diagram and weighted mean ages and 2 sigma error for the sample TP4940 (Syenogranite)

University, Hamedan, Iran. Fifteen fresh samples were selected for whole rock geochemical analyses. For this purpose, eight samples were sent to the Geological Survey and Mineral Exploration of Iran and seven samples to the Zarazma Mineral Studies Company, Iran. Major elements were analyzed by Inductively Coupled Plasma-Optical Emission Spectroscopy (ICP-OES) and trace elements by Inductively Coupled Plasma-Mass Spectroscopy (ICP-MS).

Preparation processes of zircons for U–Pb dating, such as crushing, sieving, heavy liquid and magnetic separation, hand picking under a binocular microscope, mounting on epoxy resin, and polishing were carried out at the Department of Geology, Bu-Ali Sina University, Hamedan, Iran. Forty zircon grains, 100–300 μm in size, were separated from sample TP4990 (syenogranite), and TP1011 (alkali feldspar granite). Polished grains were studied by cathodoluminescence (CL) using a scanning electron microscopy (JEOL JSM-6510LV) equipped with cathodoluminescence system (GATAN MiniCL) at Nagoya University, Japan. Forty spots from 30 zircons of sample TP4990 and 23 spots from 19 zircons of sample TP1011 were analyzed by LA-ICP-MS (Agilent 7700x) connected with a laser

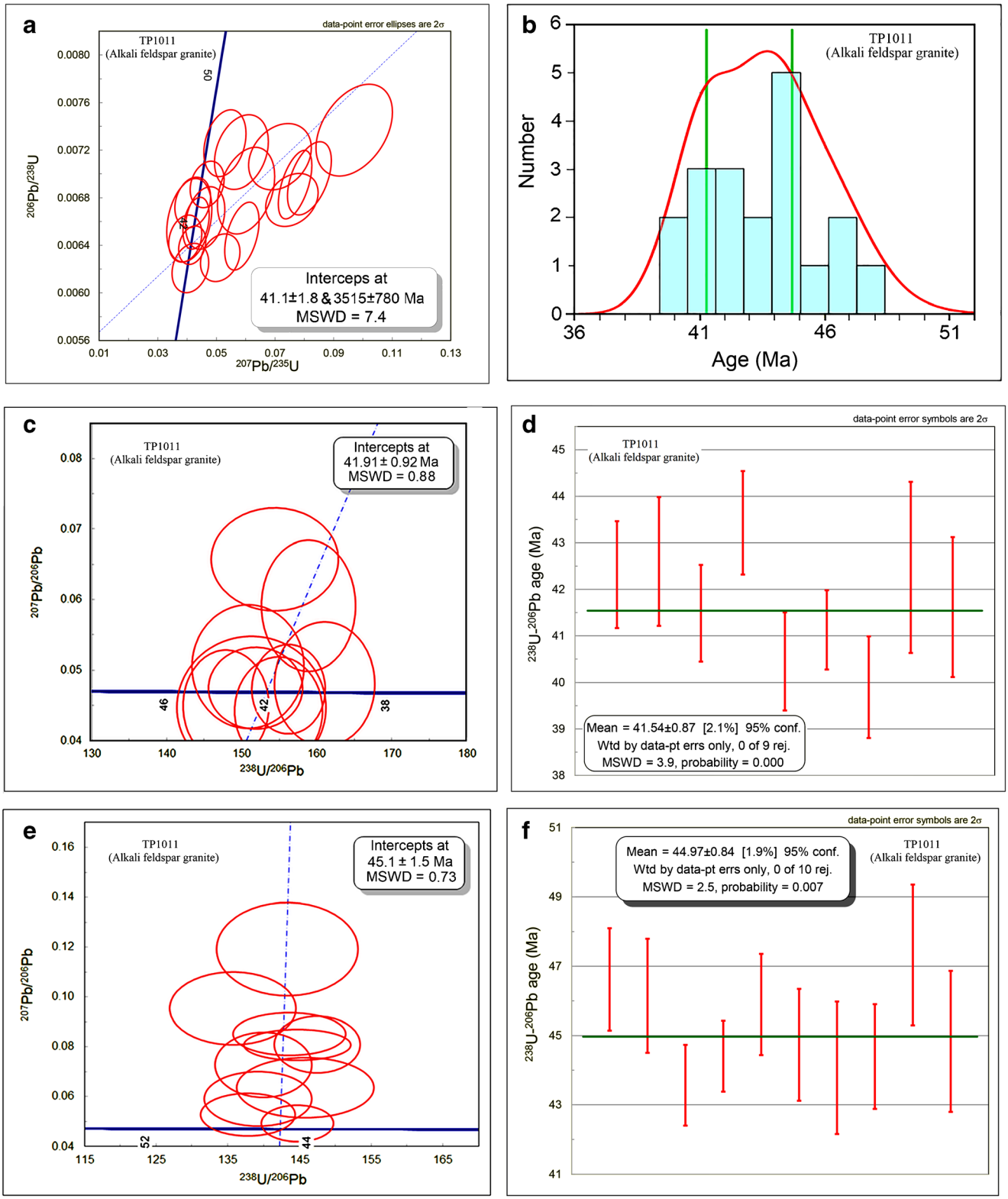

Fig. 6 Zircon U–Pb Concordia diagrams and Weighted mean ages and 2 sigma error for the sample TP1011 (Alkali feldspar granite), (b) the Age-Gaussian deconvolution diagram display two dominant age populations with peak ages of 41.3 Ma and 44.7 Ma

ablation system (NWR213 Electro Scientific Industries) at Nagoya University (Japan). ISOPLOT v. 4.15 software (Ludwig, 2012) was used for U-Pb data evaluation.

Table 2 Major and trace element concentrations of the Aliabad Daman granite, Sabzevar zone, NE Iran

Sample	TP07	TP67	TP14	TP15	TP88	TP75	TP77	TP01	TP06	TP10	TP22	TP63	TP69	TP85	TP94
Longitude(E)	59°30′ 08″	59°30′ 08″	59°33′ 58″	59°35′ 09″	59°32′ 39″	59°33′ 05″	59°34′ 46″	59°32′ 15″	59°30′ 10″	59°34′ 14″	59°29′ 37″	59°31′ 02″	59°31′ 11″	59°31′ 44″	59°31′ 29″
Latitude (N)	35°07′ 50″	35°11′ 03″	35°08′ 29″	35°08′ 12″	35°08′ 48″	35°09′ 03″	35°08′ 20″	35°09′ 50″	35°10′ 03″	35°08′ 32″	35°10′ 28″	35°10′ 09″	35°09′ 40″	35°09′ 40″	35°09′ 18″
Rock type	Granite														
SiO_2 (%)	76.10	77.00	75.80	76.20	75.40	76.20	76.30	77.34	76.93	75.87	76.06	76.35	76.72	76.46	75.83
TiO_2	0.20	0.10	0.20	0.10	0.20	0.10	0.10	0.14	0.14	0.14	0.13	0.14	0.11	0.11	0.14
Al_2O_3	12.50	12.50	12.50	12.80	12.10	12.10	12.60	11.98	11.38	12.16	12.26	11.74	11.84	11.95	12.43
FeO^T	1.06	1.00	1.06	1.26	1.00	1.60	1.26	–	–	–	–	–	–	–	–
$Fe_2O_3{}^T$	–	–	–	–	–	–	–	1.15	1.36	1.4	1.35	1.01	1.31	1.48	1.42
MnO	<0.1	<0.1	<0.1	<0.1	<0.1	<0.1	0.10	0.0068	0.0218	0.0182	0.012	0.0248	0.0173	0.0249	0.0218
MgO	0.20	<0.1	0.10	0.10	0.10	0.20	0.10	0.09	0.15	0.19	0.15	0.09	0.11	0.08	0.13
CaO	0.90	0.30	0.80	0.50	0.70	0.70	0.60	0.25	0.7	0.6	0.42	0.85	0.46	0.3	0.34
Na_2O	3.00	3.20	3.10	2.80	2.90	3.00	3.00	4.54	3.33	3.99	3.97	3.9	3.91	3.9	3.94
K_2O	4.70	4.30	4.40	4.60	4.10	4.20	4.40	3.6	4.7	4.82	4.87	4.71	4.68	4.97	4.86
P_2O_5	0.05	0.03	0.03	0.03	0.03	0.02	0.04	0.0368	0.0399	0.021	0.0323	0.0424	0.0339	0.0346	0.0323
LOI	0.75	0.85	0.95	0.81	2.77	0.92	0.38	0.75	1.32	0.83	0.8	1.2	0.86	0.75	0.93
Total	100.2	99.99	99.82	97.87	99.86	99.84	99.42	99.91	100.10	100.07	100.08	100.08	100.08	100.08	100.10
Li	–	–	–	–	–	–	–	4	3	4	4	2	3	2	2
Ni	4.15	2.19	8.95	4.72	7.1	16.53	4.95	3	6	23	15	3	3	8	2
Ga	13.86	14.05	9.74	15.06	14.07	15.87	12.63	–	–	–	–	–	–	–	–
Rb	135	120	111	125	118	138	130	65	78	108	82	68	87	70	64
Sr	69.12	37.17	64.17	37.75	60.11	51.99	81.92	55.2	63.6	142	88	62.7	51.7	46.4	61.9
Y	20.05	7.63	15.29	10.34	16.17	10.2	14.42	10.3	11.6	12.4	11.8	13.1	10.7	9	8.3
Zr	17.02	14.82	11.06	20.27	16.65	19.13	14.95	10	10	10	10	12	9	16	14
Nb	5.32	4.14	5.21	4.34	5.18	4.61	5.2	–	–	–	–	–	–	–	–
Sn	0.81	0.88	0.9	0.99	0.89	1.4	1.1	2.5	1.7	1.4	1.4	2.4	1.6	2.3	1.7
Cs	1.99	2.69	2.24	2.59	2.19	4.29	3.03	2.7	2	2.8	2.3	1.5	1.7	1.6	1.7
Ba	368	254	247	207	302	224	316	241	259	235	243	215	274	193	263
La	29.87	20.16	33.57	21.22	29.82	26.63	30.36	30	25	24	30	31	29	29	29
Ce	47.47	32.2	50.07	36.55	45.41	40.79	46.63	48	38	37	48	49	45	47	45
Pr	3.91	2.8	3.04	2.8	3.14	2.38	3.39	5.17	4.45	4.37	5.41	5.33	5.12	5.11	5.22
Nd	10.49	6.97	10.81	7.47	9.23	9.36	10.84	17	14.8	14.8	17.7	18.6	16.6	17.3	16.6
Sm	2.88	2.36	2.61	1.97	2.61	3.53	2.94	2.52	2.19	2.13	2.8	2.69	2.7	2.67	2.52
Eu	0.31	0.17	0.22	0.15	0.12	0.1	0.1	0.27	0.25	0.25	0.27	0.24	0.37	0.21	0.31
Gd	2.11	1.66	2.06	1.71	2	2.41	2.28	2.57	2.4	2.28	2.74	2.64	2.53	2.47	2.41
Tb	0.17	0.14	0.15	0.23	0.15	0.31	0.24	0.4	0.41	0.43	0.45	0.48	0.43	0.37	0.4
Tl	–	–	–	–	–	–	–	3.02	0.72	0.67	0.61	0.67	0.51	0.59	0.59
Dy	2.95	1.18	1.75	1.53	2.43	1.15	2.29	2.29	2.39	2.55	2.63	2.87	2.43	2.24	1.9
Ho	0.3	0.2	0.32	0.17	0.32	0.28	0.24	–	–	–	–	–	–	–	–
Er	1.39	0.5	0.8	0.7	0.71	0.5	0.9	1.31	1.19	1.46	1.23	1.49	1.15	0.96	0.94
Tm	0.1	0.12	0.13	0.15	0.1	0.18	0.12	0.19	0.2	0.2	0.18	0.24	0.17	0.23	0.12
Yb	1.84	0.75	1.35	1.1	1.44	1.06	1.38	1.1	1.1	1.2	1.1	1.4	1.1	1	0.9
Lu	0.12	0.14	0.18	0.15	0.1	0.17	0.13	0.18	0.2	0.2	0.19	0.23	0.17	0.15	0.15
Hf	3.38	4.11	3.67	4.27	3.59	6.45	5	1.47	1.44	1.43	1.43	1.54	1.53	1.56	1.58
Ta	0.59	1.02	0.98	1.16	0.97	1.36	0.96	0.95	0.91	1.09	1.24	1.21	1.3	1.38	0.78
Pb	23.23	22.83	33.25	26.48	25.68	22.59	11.38	12	8	7	8	6	5	4	7
Th	14.78	10.68	15.24	14.18	13.7	15.43	13.7	15.64	14.73	15.8	16.68	16.45	17.06	15.78	15.03
U	1.73	1.75	1.7	2.03	1.63	3.07	2.43	1.4	1.5	1.3	1.1	1.9	1.4	1.9	1.43

Not measured (−)

Results

Zircon U–Pb ages

Cathodoluminescence (CL) images (Fig. 4a, b) show that the zircon grains have short to medium prismatic euhedral to subhedral shape and magmatic oscillatory textures. The U–Pb data are listed in Table 1, and the concordia diagrams are plotted in Figs. 5 and 6.

Sample TP4990 (syenogranite)

Th/U ratios in the zircon grains from sample TP4990 vary between 0.32 and 2.21 with a mean value of 0.73 (Table 1). This is consistent with a magmatic origin of the grains (e.g., Xiang et al. 2011; Kirkland et al. 2015; Yakymchuk et al. 2018). Forty spots from 30 zircon grains of this sample cluster on the concordia at 39.98 ± 0.39 Ma (2σ error), MSWD = 2.6 (Fig. 5a), with a weighted mean $^{206}Pb/^{238}U$ age of 40.01 ± 0.33 Ma (2σ error),

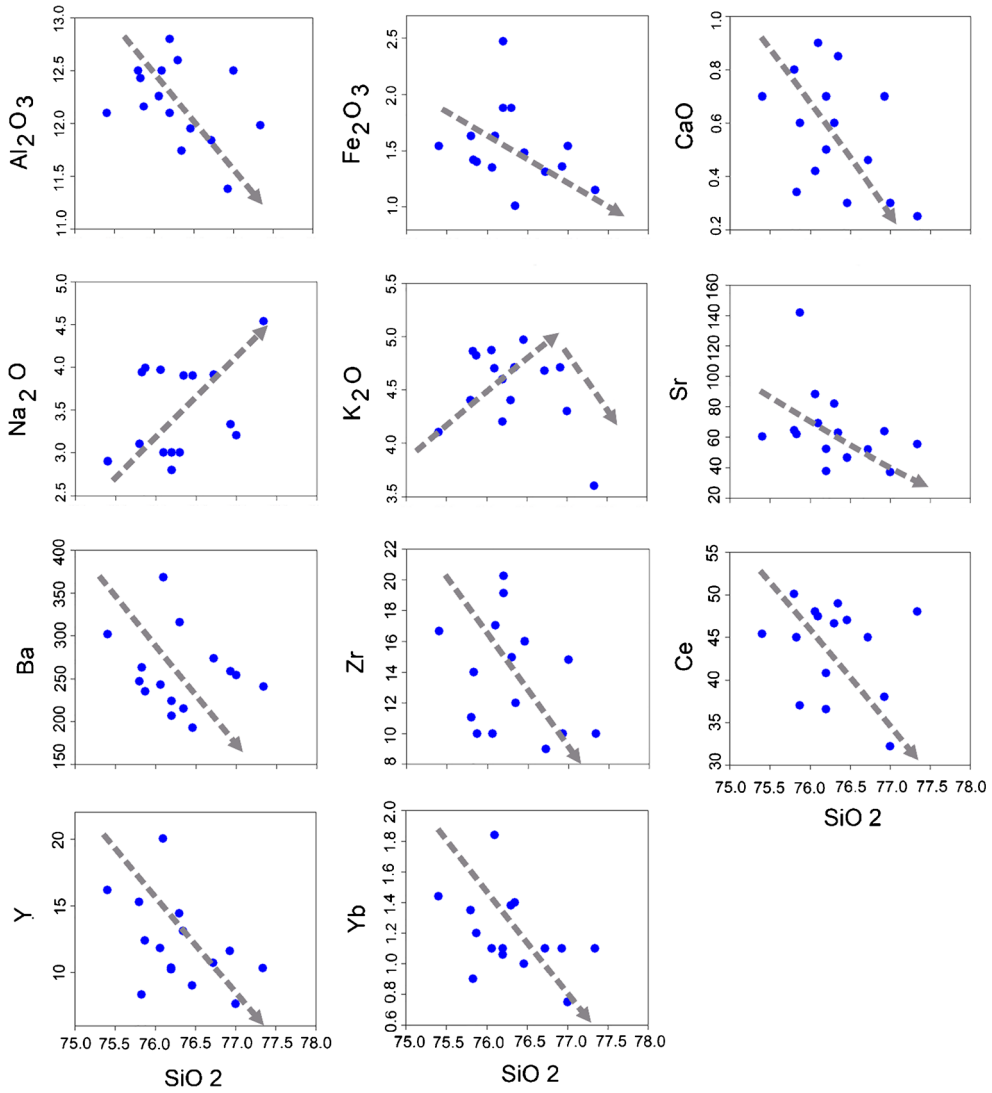

Fig. 7 Selected Harker variation diagrams for samples of the Aliabad Daman granite

MSWD = 2.5 (Fig. 5b). Interior and outer parts of most grains yield the same ages. Cores of three zircon grains yield slightly older ages of 48.5, 73.8 and 52.0 Ma (Table 1).

Sample TP1011 (alkali feldspar granite)

Twenty-three spots from 19 zircon grains were analyzed from alkali feldspar granite sample TP1011 and the U–Pb zircon analyses listed in Table 1. Nineteen zircon grains from this sample give a range of ages from *c.* 40 to 47 Ma. A discordia line through these fractions yields a lower intercept age of 41.1 ± 1.8 Ma (Fig. 6a). From the Gaussian deconvolution diagram two dominant age populations with peak ages of 41.3 Ma and 44.7 Ma are obtained (Fig. 6b). This can be taken as evidence of differences in the formation ages of the igneous rocks.

Nine spots from zircon grains of the alkali feldspar granite sample TP1011 yield a concordia (Terra-Wasserburg) age of 41.91 ± 0.92 Ma, MSWD = 0.88 (Fig. 6c), with a weighted mean $^{206}Pb/^{238}U$ age of 41.54 ± 0.87 Ma (2σ error) and an MSWD value of 3.9 (Fig. 6d). Ten spots from this sample yield a discordia (Terra-Wasserburg) age of 45.1 ± 1.5 Ma, MSWD = 0.73 (Fig. 6e), with a weighted mean $^{206}Pb/^{238}U$ age of 44.97 ± 0.84 Ma (2σ error), MSWD = 2.5 (Fig. 6f). Three spots yield an upper intercept age of *c.* 776 Ma due to presence of old inherited zircon components in the respective grains (Table 1).

Whole rock geochemistry

The results of whole rock geochemical analyses from the Aliabad Daman pluton are presented in Table 2. The rocks are commonly granitic in composition with minor variation in major elements. Silica content ranges from 75.40–77.00 wt.%., Al_2O_3 from 11.38–12.80 wt.%, CaO from 0.25–0.90 wt.%, K_2O from 3.60–4.97 wt.%, Na_2O from 2.80–3.99 wt.%, $Fe_2O_3{}^T$ from 1.01–2.47 wt.%), MgO from 0.08–0.20 wt.%, and LOI from 0.38–2.77 wt.%. In the Harker variation diagrams (Fig. 7), the samples display decreasing Al_2O_3, CaO,

Fe_2O_3, Sr, Ba, Zr, Ce, Y, Yb, increasing Na_2O, and increasing then decreasing K_2O concentrations with increasing silica.

In the REE-chondrite-normalized diagram (Fig. 8a), the samples are characterized by variable fractionation between light and heavy REE (La_N/Yb_N = 11–22) and negative Eu anomalies (Eu/Eu* = 0.1–0.4). In the primitive mantle-normalized multi-elements diagram (Fig. 8b), the samples display negative Ba, Nb, Sr, P, Zr, and Ti anomalies, relative depletion of heavy REE and enrichment of large ion lithophile elements (LILE).

In the total alkali versus silica (TAS) diagram from Middlemost (1994), all samples from Aliabad Daman pluton plot in the granite field (Fig. 9a). In the A/NK (molar $Al_2O_3/Na_2O + K_2O$) vs. A/CNK (molar $Al_2O_3/CaO + Na_2O + K_2O$) diagram all samples display metaluminous to peraluminous affinity (Fig. 9b). As shown in Fig. 9a and b, the samples have geochemical characteristic similar to those of felsic rock types from the Kashmar pluton (Shafaii Moghadam et al. 2015) and to those of the Nay pluton (Almasi et al. 2019) along the Doruneh fault zone. According to the K_2O–SiO_2 diagram of Peccerillo and Taylor (1976), the samples belong to the high-K calc-alkaline series (Fig. 9c). In the AFM triangular diagram (Fig. 9d), the granitic rocks show calc-alkaline nature.

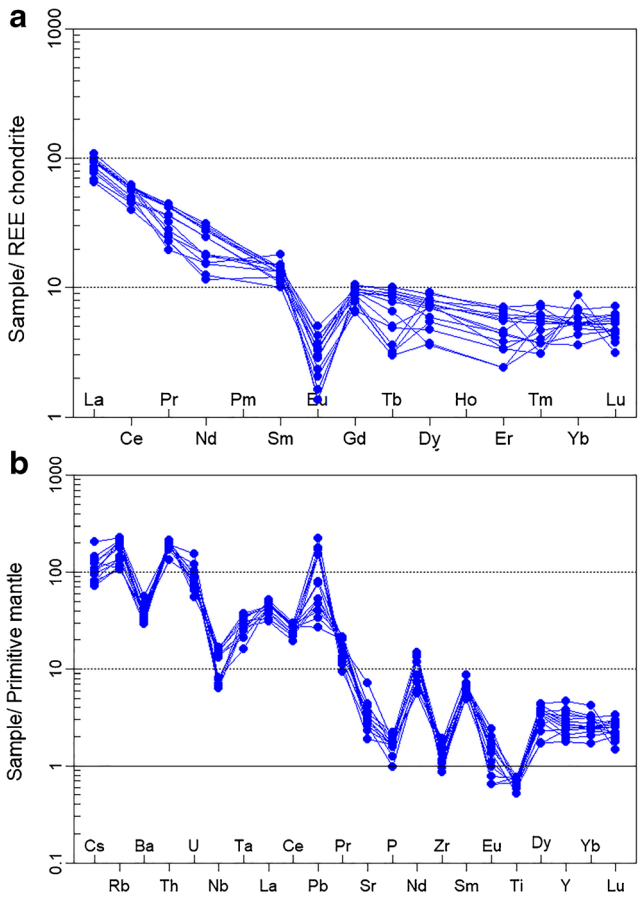

Fig. 8 **a** Chondrite normalized REE pattern for representative samples from Alabad Daman granite. **b** Primitive mantle normalized multi-elements pattern for representative samples from Alabad Daman granite. The normalized values of REE are from (Boynton 1984), the normalizing values of the multi-elements are from (Sun and McDonough 1989)

Samples from the Aliabad Daman pluton have low Sr/Y, according to the definition of Defant and Drummond (1990), but they do not have similar geochemical characteristics to adakites. In the Rb against Y + Nb diagram (Pearce et al. 1984), samples from the Aliabad Daman pluton, similar to samples from other Bartonian plutons of the Iranian structural zones plot in the volcanic arc granite (VAG) field (Fig. 10a). In the Th/Yb versus Nb/Yb diagram (Pearce 2008), the samples plot in the field of Archean crust (A) close to the data for the late-Neoproterozoic Taknar (Bornaward) granitoid complex (BGC) (Fig. 10b).

Discussion

Magma source and petrogenesis

Our results such as major-trace elements characteristics and presence of inherited zircon suggest that Aliabad Daman pluton was derived from a continental crustal source with input of mantle material. The Th/Yb versus Nb/Yb diagram (Pearce 2008) shows that the samples from the pluton have chemical properties similar to the Late-Neoproterozoic Taknar and Bornaward Granitoid Complex (BGC) (Fig. 10b). Besides, the geochemical characteristics of the Aliabad Daman pluton are comparable with felsic members of the Eocene Kashmar granitoids (Shafaii Moghadam et al. 2015), and with the Nay intrusive rocks studied by Almasi et al. (2019) (Fig. 9a, b). Sr-Nd isotopic data obtained from samples collected from the Batonin (*c.* 40 Ma) plutons along the Doruneh fault zone, southern edge of the Sabzevar suture zone, show that two end-members, i.e., an enriched mantle source and a continental crustal source were involved in magma generation (Shafaii Moghadam et al. 2015; Almasi et al. 2019) (Fig. 11).

The presence of old inherited zircons ages (e.g., 623 Ma) in the Aliabad Daman pluton suggests that melts of the Cadomian crust played a role in the generation of the magma. Also, the presence of old inherited zircons with an age of *c.* 640 Ma in felsic members of the Kashmar granitoids from the Zabzevar zone (Shafaii Moghadam et al. 2015) support the assimilation of the Cadomian crust during Bartonian magmatism. Hence, it seems that the magmas of the Aliabad Daman pluton were generated by partial melting of material from the continental crust and the lithospheric mantle.

From the Zr/Nb versus Zr diagram (Shen and Pan 2013) and the Dy/Yb versus Dy, La/Yb versus La diagrams (Gao et al. 2007), it can be inferred that partial melting played a more important role than fractional crystallization in the generation of the Aliabad Daman magma (Fig. 12a–c). However, in Harker variation diagrams (Fig. 7), the samples display decreasing Al_2O_3, CaO, FeO, Sr, Ba, Zr, and Y and increasing Na_2O, K_2O concentrations with increasing silica. This

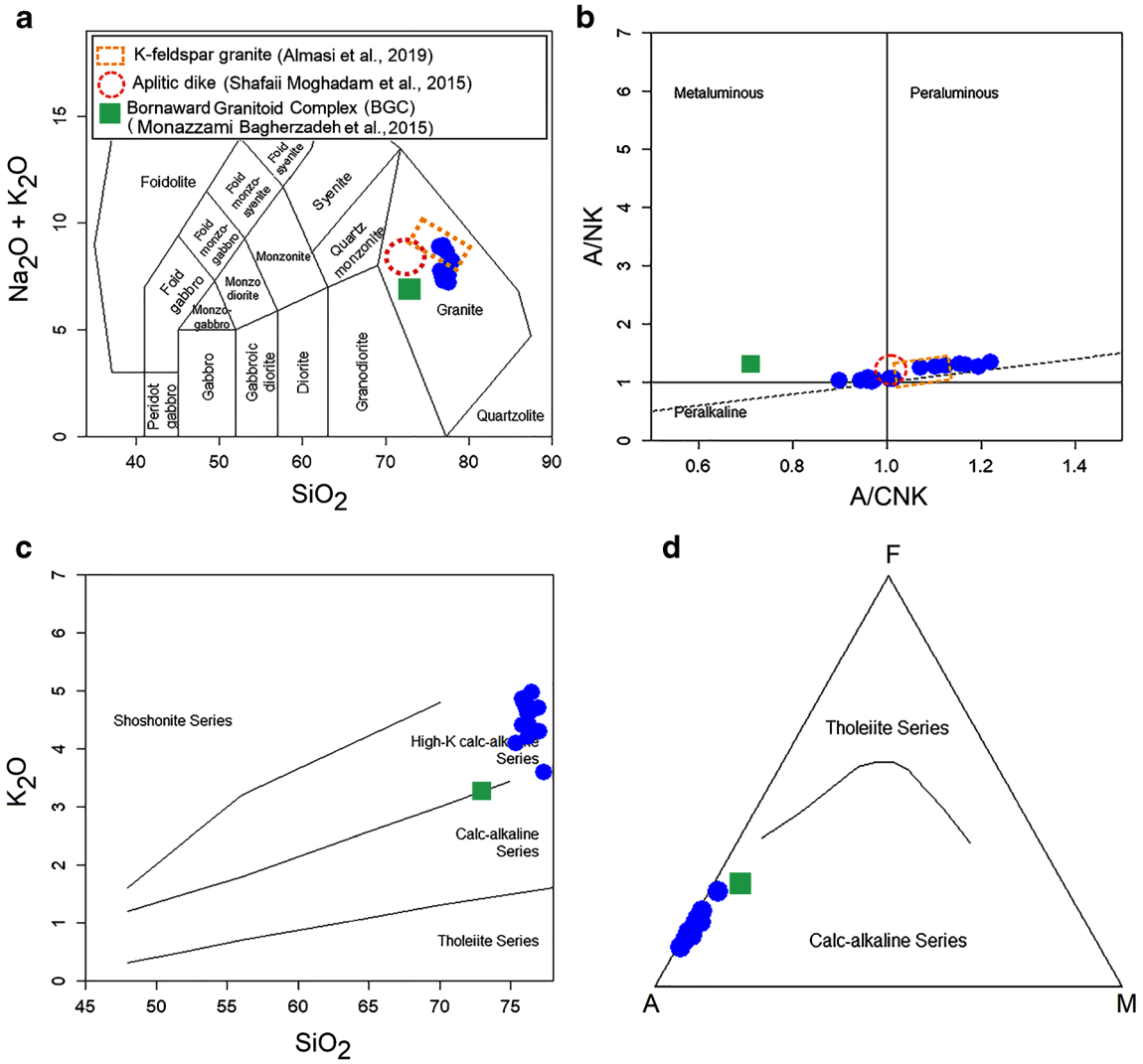

Fig. 9 **a** Total alkalis versus SiO2 diagram for classification of the Aliabad Daman rocks (after Middlemost 1994). Compositional field for the Bartonian (~40 Ma) felsic rocks in the Sabzevar zone (yellow and red dashed line) and source rock of the Late-Neoproterozoic Taknar and Bornaward Granitoid Complex (BGC) (green square) respectively are from (Almasi et al. 2019; Shafaii Moghadam et al. 2015; Monazzami Bagherzadeh et al. 2015). **b** A/NK (molar Al2O3/Na2O + K2O) vs. A/CNK (molar Al2O3/CaO + Na2O + K2O) diagram. **c** K2O–SiO2 diagram. **d** AFM diagram. A (Na2O + K2O), F (FeO + Fe2O3), M (MgO) (Irvine and Baragar 1971) diagram

variation can be ascribed to the fractionation of Ca-rich plagioclase, Fe oxides and zircon during crystallization. Sr, Ba, and Y are compatible in Ca-rich plagioclase; consequently, Sr, Ba, and Y decreased due to fractionation of Ca-rich plagioclase.

Geodynamic setting and geochronological characteristics

U-Pb zircon ages for Cretaceous and Paleogene extrusive and intrusive rocks of the Sabzevar Ophiolitic Suture Zone (SOSZ) are summarized in Table 3, and the resulting age spectrum is shown in Fig. 13. From the middle Jurassic to early Cretaceous extensional tectonics prevailed in the oceanic realms around the Central Iranian Microcontinent (e.g., Lindenberg et al. 1984; Sengör 1990). The Sabzevar oceanic crust started to form during the early Jurassic and reached its maximum extension during the early Cretaceous (e.g., Stöcklin 1974; Omrani et al. 2018). The presence of continental alkaline basalts, dikes, and sills in the lower members of the Shemshak Formation (e.g., Annells et al. 1975; Ghasemi and Jamshidi 2012) points to the likelihood of extensional tectonics in the early Jurassic time in the Sabzevar zone. The presence of sandstone, siltstone, shale and claystone in the early Jurassic Shemshak Formation (Fig. 2) is further evidence for the existence of an oceanic environment and for extensional tectonics in the Sabzevar zone. Thus, the generation of the Sabzevar ocean as a back–arc domain in the Neotethyan

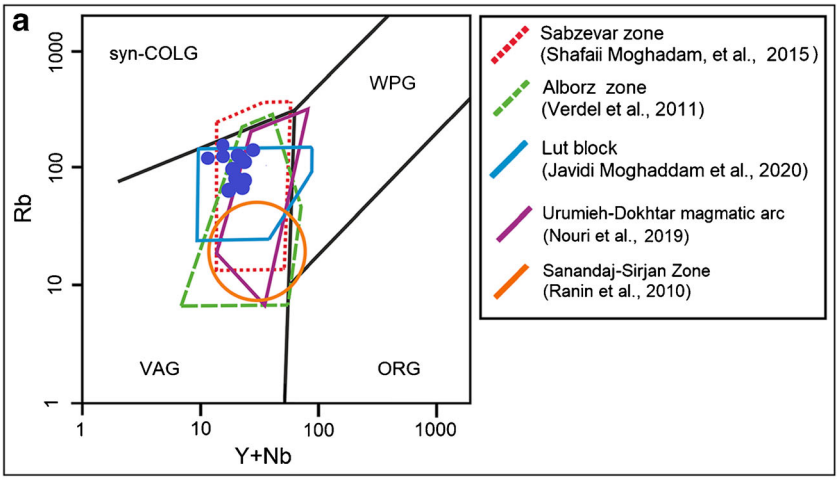

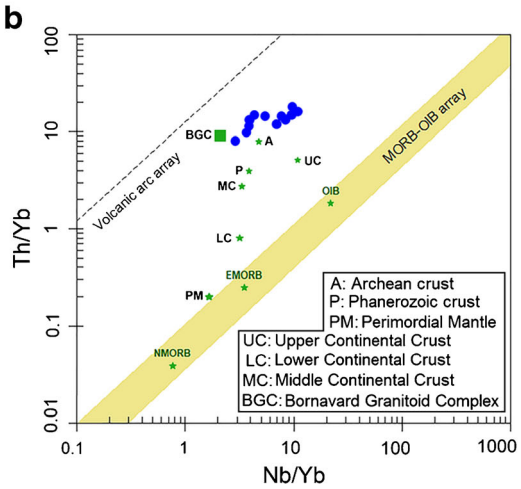

Fig. 10 **a** Rb vs. Y + Nb diagram (Pearce et al. 1984) for samples from Aliabad Daman granite, Compositional field for the Bartonian (~40 Ma) magmatism of the Sabzevar zone, Alborz zone, Lut block, Urumieh-Dokhtar magmatic arc and Sanandaj-Sirjan zone respectively are from Shafaii Moghadam et al. (2015), Verdel et al. (2011), Javidi Moghaddam et al. (2020), Nouri et al. (2019) and Ranin et al. (2010). **b** Th/Yb vs. Nb/Yb diagram (Pearce et al., 2008) of the Aliabad Daman granitic samples and its source rock (BGC)

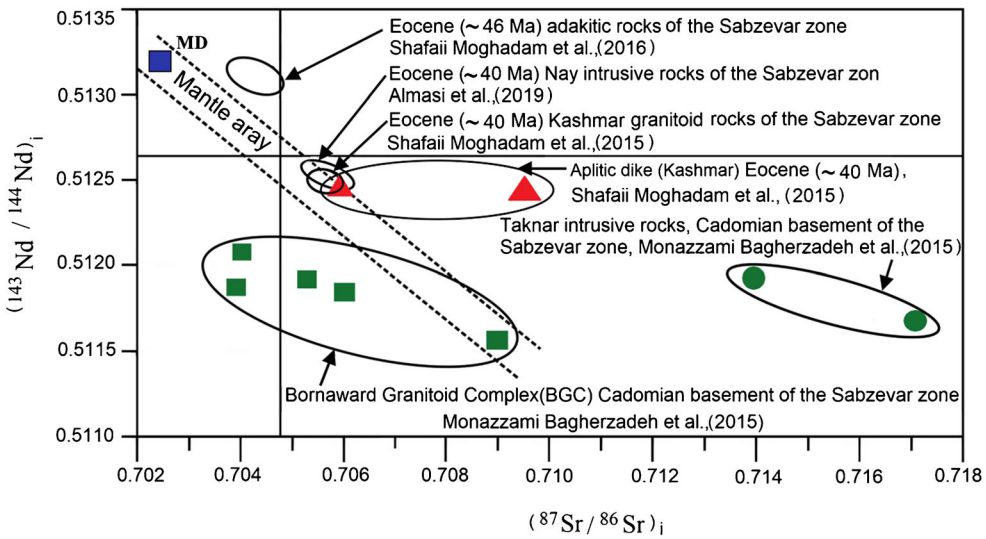

Fig. 11 Initial 143Nd/144Nd vs. (87Sr/86Sr)i for Eocene (~ 40 Ma, Bartonian time) magmatic rocks of the Zabzevar zone along the Doruneh fault zone compared with Eocene (~ 46 Ma, Lutetian time) adakitic rocks and Late-Neoproterozoic Taknar and Bornaward Granitoid Complex (BGC) from Zabzevar zon. Data for Eocene (~ 46 Ma, Lutetian time) adakitic rocks, from Shafaii Moghadam et al., (2016); data for Nay intrusive rocks, from Almasi et al., (2019); data for Kashmar granitoid rocks, from Shafaii Moghadam et al., (2015); data for Taknar and Bornaward Granitoid Complex (BGC), from Monazzami Bagherzadeh et al., (2015)

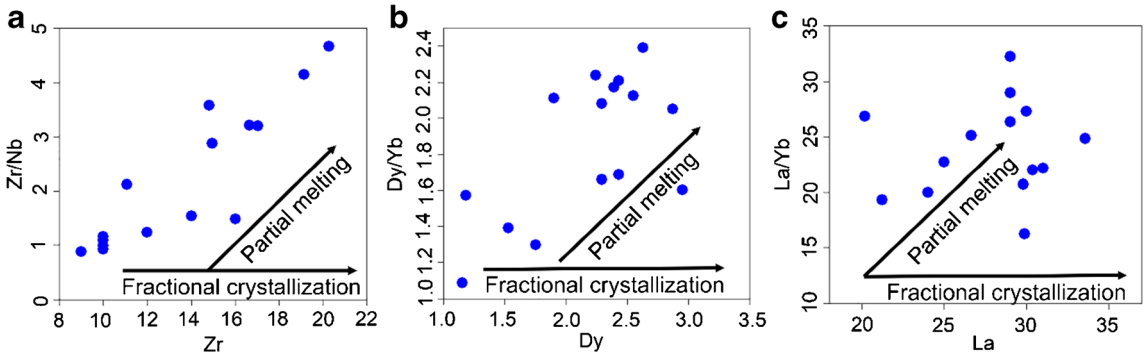

Fig. 12 **a** Zr/Nb versus Zr diagram (Shen and Pan 2013), **b**, **c** La/Yb versus La and Dy/Yb versus Dy diagrams (Gao et al. 2007) display that partial melting has important role rather than fractional crystallization in Aliabad Daman Granite

subduction system probably started from middle Jurassic by rifting and sedimentation of clastic sediments (Skemshak Formation) in a continental shallow basin. It was completed by deposition of pelagic limestone associated with volcanic rocks during middle Cretaceous (Aptian) times (*c.* 115 Ma).

It has been frequently stated that the Sabzevar Ocean was created in the back–arc domain of the Neotethyan ocean during Mesozoic time (e.g., Sengör et al. 1988; Sengör 1990; McCall 1997; Bagheri and Stampfli 2008; Rossetti et al. 2010; Jamshidi et al. 2015a; Shafaii Moghadam et al. 2015, 2016, 2019; Mazhari et al. 2019; Kazemi et al. 2019; Almasi et al. 2019; Rahmani et al. 2020). Numerous investigators argue that the magmatic rocks of the Sabzevar zone such as mantle ophiolite sequence, mafic and ultramafic units of the ophiolite sequence, volcano-sedimentary sequence (pelagic limestone), crustal plutonic rocks and extrusive rocks were generated in a supra-subduction setting (e.g., Khalatbari Jafari et al. 2013a, b; Shafaii Moghadam et al. 2014; Rahmani et al. 2017; Omrani et al. 2018; Omrani 2018; Kazemi et al. 2019). It was also stated that the Sabzevar ophiolites formed as island arc tholeiites (IAT) in an intra-oceanic arc setting and in a supra-subduction system (e.g., Shojaat et al. 2003; Rossetti et al. 2010; Khalatbari Jafari et al. 2013a, b; Shafaii Moghadam et al. 2014; Omrani et al. 2018; Rahmani et al. 2017; Omrani 2018; Kazemi et al. 2019; Rahmani et al. 2020).

U-Pb dating of zircon and titanite from felsic rocks (tonalite / trondhjemite) of the Sabzevar ophiolite indicates a range of ages from 115 to 99 Ma. These rocks coexist with garnet-clinopyroxene residues (granulite) that formed by melting of mafic rocks (Rossetti et al. 2010). *C.* 93 Ma old I-type granitoids are present in the Arghash region (Alaminia et al. 2013). Petrological and geochronological data on other rock units of the ophiolite sequence from the Sabzevar zone such as plagiogranite, gabbro, tonalite, and diabasic dike within the peridotite members show that they formed during upper Cretaceous time (100–78 Ma) from a depleted mantle source (Shafaii Moghadam et al. 2014, 2019). The formation of basaltic andesites (c. 93 Ma) from the Kabudan area (Mazhari et al. 2019) and granitic rocks (*c.* 102 Ma) from the southern edge of Sabzevar basin (Kazemi et al. 2019) is related to subduction zone magmatism. Thus, it can be concluded that an intra-oceanic arc setting existed in the Sabzevar structural zone during Albian times. We propose that a supra-subduction system existed in the Sabzevar back-arc basin during lower Cretaceous Aptian time. Also, the southern flank of the Sabzevar oceanic crust started to subduct beneath its northern side at *c.* 110 Ma (pre-Albian). Based on results reported by Rossetti et al. (2010), Shafaii Moghadam et al. (2014), Kazemi et al. (2019), Mazhari et al. (2019) and Shafaii Moghadam et al. (2019), magmatic activity related to a supra-subduction system continued until the upper Cretaceous (Campanian) (Table 3, Fig. 13).

It was postulated that the Sabzevar ocean closed during the transition from Paleocene to Eocene time (*c.* 57 Ma, Thanetian) contemporaneous to the suturing between Iran and Arabia (e.g., Davoudzadeh 1972; Lensch et al. 1977; Mazhari et al. 2009; Delaloye and Desmons 1980; 1981; Spies et al. 1983; Baroz et al. 1984; Sengör et al. 1988; Arvin and Robinson 1994; Stampfli and Borel 2002; Shojaat et al. 2003; Omrani et al. 2008; Rossetti et al. 2010; Agard et al. 2011; Jamshidi et al. 2018; Kazemi et al. 2019). As shown in Fig. 14, Eocene magmatic activity of the Sabzevar zone is contemporaneous with magmatic activity in the central Alborz zone (Verdel et al. 2011).

For a long time period, from upper Cretaceous time (*c.* 75 Ma, Campanian) to upper Paleocene time (*c.* 57 Ma, Thanetian) no magmatic activity occurred in the Sabzevar zone (Fig. 13). During this time, closure of the Sabzevar Ocean only occurred by shorting and thickening of oceanic crust and lithospheric mantle. This interval possibility corresponds to the subsidence of intra-oceanic subduction of the Sabzevar basin (*c.*75 Ma, Campanian) and to the start of collision between the central Iranian microcontinent (CIM) and the Turan block. Tadayon et al. (2018) depict a tectono-

Table 3 Summary of zircon/titanite U-Pb and ^{40}Ar-^{39}Ar age data from the Sabzevar zone, NE Iran

Location	Lithology	Method	Age (Ma)	References
Delbar (NW Sabzevar city)	Ophiolite (Mafic granulite	LA-ICPMS zircon U–Pb	107.4±2.4	Rossetti et al. 2010
	Ophiolite (Mafic granulite	LA-ICPMS titanite U–Pb	109.4±2.3	
Arghash (SE Sabzevar city)	Granodiorite	LA-ICPMS zircon U–Pb	92.8±1.3	Alaminia et al. 2013
	Granite		55.4±2.3	
	Hornblende Diorite		553.5±6.1	
Soltan Abad (NE Sabzevar city)	Granitoid (Adakitic)	LA-ICPMS zircon U–Pb	57.9±2.4	Rossetti et al. 2014
	Garnet-Amphibolite (leucosome)		57.34±0.46	
	Granitoid (Adakitic)	Muscovite-$^{40}Ar/^{39}Ar$	50.0±0.6 (Cooling age)	
	Garnet-Amphibolite	Amphibole-$^{40}Ar/^{39}Ar$	50.9±1.8 (Cooling age)	
N- Sabzevar city	Tonalite dike in mantle	TIMS-U-Pb	99.92±0.12	Shafaii Moghadam et al. 2014
	Plagiogranite in sheeted dike		90.16±0.12	
	Plagiogranite-Torbat Heydarieh		98.40±0.29	
	Plagiogranite in gabbro		77.82±0.28	
S- Sabzevar city	Dacite/Rhyolite (Adakitic)	SHIRMP-U-Pb	48.01±0.62	Jamshidi et al. 2015b
Kashmar (SE-Sabzevar city)	Monzogranite	LA-ICPMS zircon U–Pb	41.09±0.30	Shafaii Moghadam et al. 2015
	Aplitic dike		40.13±0.53	
	granodiorite		39.87±0.47	
	Granodiorite		40.48±0.64	
	Micro-granodioritic enclave		40.54±0.40	
NW-Sabzevar city	Andesitic dome (Adakitic)	LA-ICPMS zircon U–Pb	45.32±0.64	Shafaii Moghadama et al. 2016
	Andesitic dome (Adakitic)		46.77±0.74	
	Andesitic dome (Adakitic)		46.48±0.85	
	Rhyolitic rocks (Adakitic)		46.75±0.26	
	Andesitic rocks (Adakitic)		46.44±0.11	
NE-Rashtkhar	Syenite	LA-ICPMS zircon U–Pb	40±0.94	Alizadeh et al. 2017
NW-Sabzevar city	Rhyolite (Adakitic)	SHIRMP-U-Pb	46.62±0.89	Jamshidi et al. 2018
	Rhyolite (Adakitic)		48.01±0.62	
	Rhyolite (Adakitic)		49.09±0.77	
	Rhyolite (Adakitic)		43.09±0.59	
	Andesite (Adakitic)		45.51±0.97	
	Andesite (Adakitic)		44.77±0.74	
	Dacite (Adakitic)		44.54±0.98	
	Andesite (Adakitic)		47.24±0.88	
Nay (NE-Sabzever city)	Quartz monzonite	TIMS-U-Pb	40.21±0.30	Almasi et al. 2019
SW-Sabzevar city	Gabbrodiorite	LA-ICPMS zircon U–Pb	75.65±0.52	Kazemi et al. 2019
	Granite		98.03±0.68	
	Granite		100.44±0.95	
	Granite		101.9±1.0	
	Rhyolite		99.2±2.5	
Kaboodan (SE-Sabzevar city)	basaltic andesite	LA-ICPMS zircon U–Pb	93.45±0.42	Mazhari et al. 2019
	Andesite		92.04±0.99	
	Acidic tuff		87.36±0.86	
	Dacite		81.88±0.98	
	Andesitic tuff		75.18±0.50	
	Hornblende gabbro		98.55±0.80	

Table 3 (continued)

Location	Lithology	Method	Age (Ma)	References
	Hornblende gabbro		98.65±0.78	
	Granitoid dike		81.48±0.54	
	Granitoid (Taknar area)		80.12±0.94	
	Garnitoid		81.37±0.74	
Torbat-e-Heydarieh	Ophiolite-Plagiogranitic dike	SHIRMP-U-Pb	99.32±0.72	Shafaii Moghadam et al. 2019
	Ophiolite- Gbbroic dike		96.7±2.1	
	Ophiolite- Plagiogranite		91.90±0.33	
	Ophiolite- Plagiogranite		97.00±1.3	
	Ophiolite- Diabasic dike		97.1±1.2	
	Ophiolite- Plagiogranitic dike		97.9±0.6	
Aliabad Daman (NE-Rashtkhar city)	Granite	LA-ICPMS zircon U–Pb	40.01±0.33	Present study
			41.1±1.8	
			41.54±0.87	
			44.97±0.84	

stratigraphic evolutionary model of the Doruneh fault region for this time period.

Middle Eocene igneous rocks in the Sabzevar structural suture zone can be divided to two main groups, (i) adakitic igneous rocks of Lutetian (*c*. 47 Ma) age (Alaminia et al. 2013; Rossetti et al. 2014; Jamshidi et al. 2015b; Shafaii Moghadam et al., 2016; Jamshidi et al. 2018), and (ii) calc-alkaline igneous rocks without adakitic affinities of Bartonin (*c*. 40 Ma) age (Shafaii Moghadam et al. 2015; Alizadeh et al. 2017; Almasi et al. 2019; this study). From middle Eocene to present time, extensive alkaline and calc-alkaline volcanic rocks, unrelated to subduction zone processes, were formed in respond to shortening and thickening of the central Iran microplate (Berberian and King 1981). This petrogenetic model is compatible with present-day crustal thicknesses and a gravimetric Moho depth of 47 km in the Sabzevar zone reported by Dehghani and Makris (1983), an Eocene initiation age of the Doruneh fault zone (Javadi et al. 2013), and the tectono-stratigraphic evolutionary model for the Doruneh fault region (Tadayon et al. 2017, 2018). Magmatism occurred after the cessation of subduction (*c.* 57 Ma, Thanetian) by melting of the detached slab of oceanic crust (MORB), and upwelling of the asthenosphere. Therefore, shortening and thickening of the continental crust and the lithospheric mantle, delamination of the lower crust and the lithospheric mantle, and heating by asthenospheric upwelling played important roles in the production of the middle Eocene (*c*. 45 Ma, Lutetian) and the younger granitoids such as the Aliabad Daman pluton and the initiation of the Doruneh fault zone (Fig. 15).

Conclusions

Based on whole rock geochemical data, the Aliabad Daman pluton represents a metaluminous to peraluminous magma body belonging to the high-K calc-alkaline series.

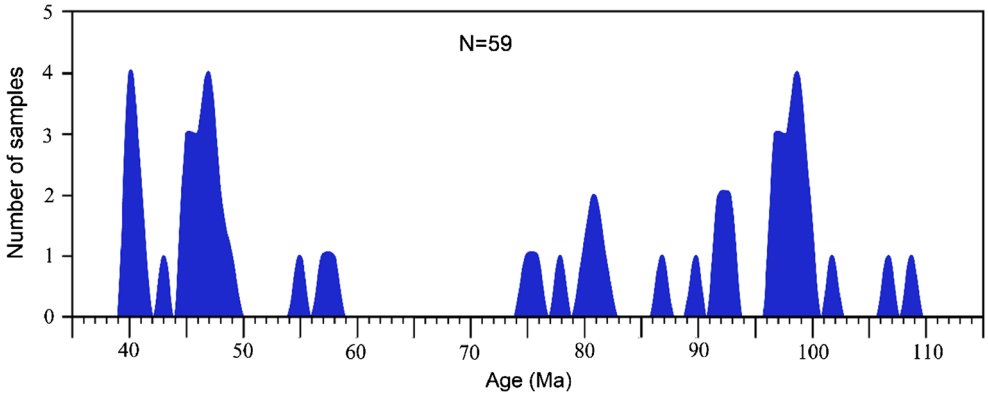

Fig. 13 Spectrogram for zircon/titanite U-Pb and 40Ar-39Ar age data from the Sabzevar Ophiolitic Suture Zone (SOSZ). N: Number of published age data for the samples collected from the SOSZ. Data sources are summarized in the Table 3

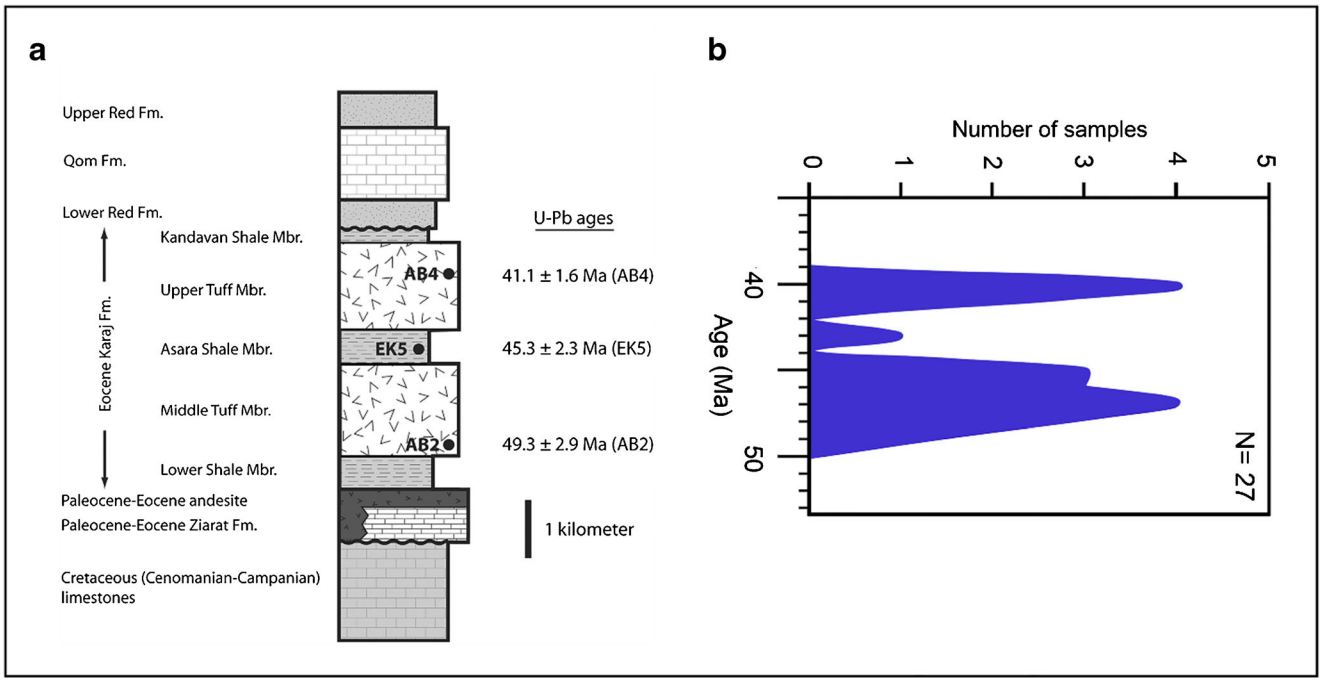

Fig. 14 Correlation of the magmatic activities in the Sabzevar ophiolitic suture zone and Alborz zone after closing of the Sabzevar Ocean, from upper Paleocene (~ 57 Ma). (**a**) Stratigraphy of the Chalus Road area and geochronological results of magmatic activities are from Verdel et al. (2011). (**b**) Spectrogram of the magmatic activities in the Sabzevar ophiolitic suture zone is taken from Fig. 13

Compositional variations of major and trace elements can be mainly related to the partial melting process. The U–Pb dating results show that the magmas crystallized 45–40 Ma ago. Geochemical characteristics, the presence of inherited zircon, and the combination of new results with previous studies suggest that the Aliabad Daman pluton formed by melting of material from the continental crust and the lithospheric mantle.

Middle Eocene igneous rocks in the Sabzevar structural suture zone comprise a group of the adakitic rocks of Lutetian (c. 47 Ma) age and a group of rocks without adakitic affinities of Batonin (*c*. 40 Ma) age. From upper Cretaceous to upper Paleocene (*c.* 75 to 57 Ma) no magmatic activity occurred in the Sabzevar zone. During this period, closing events within the Sabzevar Ocean only occurred by shorting and thickening of the oceanic crust and the lithospheric mantle.

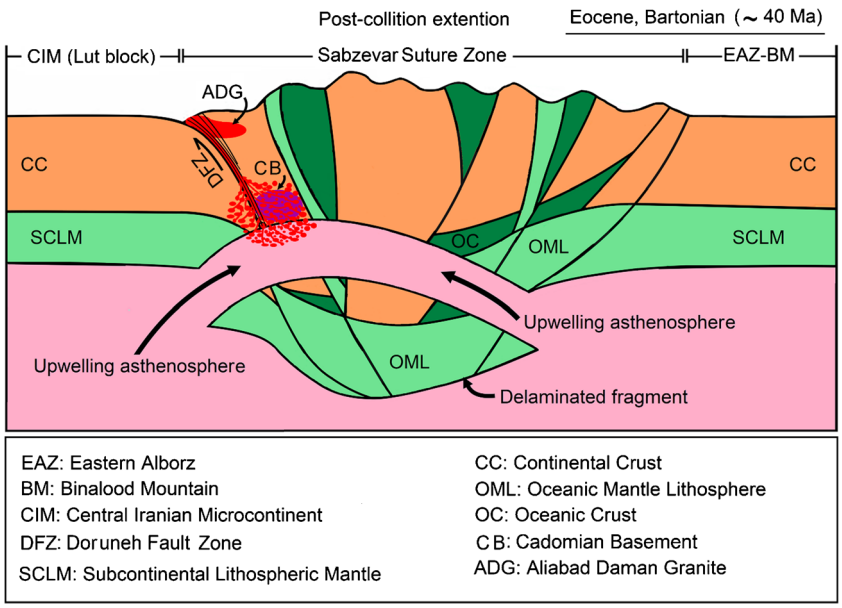

Fig. 15 Schematic model showing the generation of the Aliabad Daman granitic body. Occurrence of post-collision extension, extensional collapse of the Sabzevar ophiolitic suture zone, asthenosphere upwelling, delamination of the lower crust and mantle lithosphere, Doruneh fault zone activities, and generation of the fault related calc-alkaline igneous rocks without adakitic affinities of the Aliabad Daman granite at Middle Eocene, Bartonian time (~ 40 Ma)

Delamination of the lower crust and the lithospheric mantle followed by upwelling of hot asthenosphere played an important role in the production of the Aliabad Daman pluton. Tectonic activity along the Doruneh fault zone and the extensional collapse of the crust also contributed to the generation and emplacement of this pluton.

Acknowledgments This study is a part of Mohammad Amin Shakouri master thesis. The authors would like to thank Prof. Hossein Azizi and Prof. Yoshihiro Asahara for support during BSE-CL imaging and LA-ICPMS analyses. Also, we are thankful for editing by Prof. Lorence G. Collins and Prof. W. Siebel of the manuscript.

References

Agard P, Omrani J, Jolivet L, Whitechurch H, Vrielynck B, Spakman W, Monié Meyer B, Wortel MJR (2011) Zagros orogeny: a subduction-dominated process. Geol Mag 148:692–725

Alaminia Z, Karimpour MH, Homam SM, Finger F (2013) The magmatic record in the Arghash region (northeast Iran) and tectonic implications. Int J Earth Sci (Geol Rundsch) 102:1603–1625

Alizadeh E, Ghadami G, Esmaeily D, Ma Ch, Lentz DR, Omrani J, Golmohammadi A (2017) Origin of 1.8 Ga zircons in Post Eocene mafic dikes in the Roshtkhar area, NE Iran. Int Geol Rev 60:1855–1882

Almasi A, Karimpour MH, Arjmandzadeh R, Santos JF, Ebramimi Nasrabadi K (2019) Zircon U-Pb geochronology, geochemistry, Sr-Nd isotopic compositions, and tectonomagmatic implications of Nay (NE Iran) postcollisional intrusives in the Sabzevar zone. Turk J Earth Sci 28:372–397

Annells RN, Arthurton RS, Bazely RA, Davis RG (1975) "Explanatory text of the Qazvin and Rasht quadrangles map (1:250000)", Geological Survey of Iran. Report No. E3, E4. (1975) 94 pp.

Arvin M, Robinson T (1994) The petrogenesis and tectonic setting of lavas from the Baft ophiolitic melange, southwest of Kerman, Iran. Can J Earth Sci 31:824–834

Bagheri S, Stampfli GM (2008) The Anarak, Jandaq and Posht-e-Badam metamorphic complexes in central Iran, New geological data, relationships and tectonic implications. Tectonophysics 451:123–155

Baroz F, Macaudiere J, Montigny R, Noghreyan M, Ohnenstetter M, Rocci G (1984) Ophiolites and related formations in the central part of the Sabzevar range (Iran) and possible geotectonic reconstructions. Neues Jahrb Geol Palaontol Abh 168:358–388

Berberian M, King GCP (1981) Towards a paleogeography and tectonic evolution of Iran. Can J Earth Sci 18:210–265

Bonnet G, Agard P, Whitechurch H, Fournier M, Angiboust S, Carona B, Omrani J (2020) Fossil seamount in southeast Zagros records intraoceanic arc to back-arc transition: New constraints for the evolution of the Neotethys. Gondwana Res 81:423–444

Boynton WV (1984) Cosmochemistry of the rare earth elements: meteorite studies. In: Henderson, (Ed.), Rare Earth Element Geochemistry, Elsevier, Amsterdam, pp. 63–114,

Davoudzadeh M (1972) Geology and petrography of the area north of Nain, Central Iran. Tehran, Geological Survey of Iran Report no. 39, 89 pp.

Defant MJ, Drummond MS (1990) Derivation of some modern arc magmas by melting of young subducted lithosphere. Nature 347: 662–665

Dehghani GA, Makris T (1983) The gravity field and crustal structure of Iran. Geodynamic project (Geotraverse) in Iran, Geological Survey of Iran, Final Report number 51: 51–68

Delaloye M, Desmons J (1980) Ophiolites and melange terranes in Iran: A geochronological study and its paleotectonic implications. Tectonophysics 68:83–111

Gao YF, Hou ZQ, Kamber BS, Wei RH, Meng XJ, Zhao RS (2007) Adakite-like porphyries from the southern Tibetan continental collision zones: evidence for slab melt metasomatism. Contrib Mineral Petrol 53:105–120

Ghasemi H, Jamshidi K (2012) Geochemistry, petrology and proposed tectonomagmatic model for generation of alkaline basic rocks in the base of the Shemshak Formation, the eastern Alborz zone. Iranian Journal of Crystallography and Mineralogy 19:699–714

Irvine TN, Baragar WRA (1971) A guide to the chemical classification of the common volcanic rocks. Can J Earth Sci 8:523–548

Jamshidi K, Ghasemi H, Troll SM, Dahren B (2015a) Magma storage and plumbing of adakite-type post-ophiolite intrusions in the Sabzevar ophiolitic zone, northeast Iran. Solid Earth 6:1–24

Jamshidi K, Ghasemi H, Miao L (2015b) U-Pb age dating and determination of source region composition of postophiolite adakitic domes of Sabzevar. Iranian journal of Petrology 6:121–139

Jamshidi K, Ghasemi H, Laicheng M, Sadeghian M (2018) Adakite magmatism within the Sabzevar ophiolite zone, NE Iran: U-Pb geochronology and Sr-Nd isotopic evidences. Geopersia 8:111–130

Javadi HR, Ghassemi MR, Shahpasandzadeh M, Guest B, Ashtiani ME, Yassaghi A, Kouhpeyma M (2013) History of faulting on the Doruneh Fault System: implications for the kinematic changes of the Central Iranian Microplate. Geol Mag 150(4):651–672

Javidi Moghaddam M, Karimpour MH, Malekzadeh Shafaroudi A, Santos JF, Corfu F (2020) Middle Eocene magmatism in the Khur region (Lut Block, Eastern Iran): implications for petrogenesis and tectonic setting. Int Geol Rev. https://doi.org/10.1080/00206814.2019.1708815

Kazemi Z, Ghasemi H, Tilhac R, Griffin W, Shafaii Moghadam H, O'Reilly S, Mousivand F (2019) Late Cretaceous subduction-related magmatism on the southern edge of Sabzevar basin, NE Iran. J Geol Soc Lond 176(3):530. https://doi.org/10.1144/jgs2018-076

Khalatbari Jafari M, Babaie HA, Mirzaie M (2013a) Geology, petrology and tectonomagmatic evolution of the plutonic crustal rocks of the Sabzevar ophiolite, NE Iran. Geol Mag 150(50):862–884

Khalatbari Jafari M, Babaie HA, Gani M (2013b) Geochemical evidence for late cretaceous marginal arc-to-backarc transition in the Sabzevar ophiolitic extrusive sequence, Northeast Iran. J Asian Earth Sci 70–71:209–230

Kholghi Khosraghi MH (1996a) Geological map 1: 100,000 of Dolatabad , prepared by Geological Survey of Iran

Kholghi Khosraghi MH (1996b) geological map 1: 100,000 of Torbat-e-Heydarieh prepared by Geological Survey of Iran

Kirkland CL, Smithies RH, Taylor RJM, Evans N, McDonald B (2015) Zircon Th/U ratios in magmatic environs. Lithos 212:397–414

Lensch G, Mihn A, Alavi-Tehrani N (1977) Petrography and geology of the ophiolite belt north of Sabzevar (Khorasan), Iran. Neues Jahrb Geol Palaeontol Abh 131:156–178

Lindenberg HG, Görler K, Jacobshagen V, Ibbeken H (1984) Post-Paleozoic stratigraphy, structure and orogenetic evolution of the southern Sabzevar Zone and the Taknar Block (Khorassan, NE Iran). Neues Jahrbuch fiir Geologie und Palitontologie, Abhandlungen 168:287–326

Mazhari SA, Bea F, Amini S, Ghalamghash J, Molina JF, Montero P, Scarrow JH, Williams IS (2009) The Eocene bimodal Piranshahr massif of the Sanandaj–Sirjan Zone, NW Iran. A marker of the end of the collision in the Zagros Orogen. J Geol Soc Lond 166: 53–69

Mazhari SA, Klötzli U, Safari M (2019) Petrological investigation of Late Cretaceous magmatism in Kaboodan area, NE Iran: Evidence for an active continental arc at Sabzevar zone. Lithos 348–349:105183

McCall GJH (1997) The geotectonic history of the Makran and adjacent areas of southern Iran. J Asian Earth Sci 15:517–531

Middlemost EA (1994) Naming materials in the magma/igneous rock system. Earth-Sci Rev 37:215–224

Monazzami Bagherzadeh R, Karimpour MH, Lang Farmer G, Stern CR, Santos JF, Rahimi B, Heidarian Shahria MR (2015) U–Pb zircon geochronology, petrochemical and Sr–Nd isotopic characteristic of Late Neoproterozoic granitoid of the Bornaward Complex (Bardaskan-NE Iran). J Asian Earth Sci 111:54–71

Nouri F, Azizi H, Stern RJ, Asahara Y, Khodaparast S, Madanipour S, Yamamoto K (2019) Zircon U-Pb dating, geochemistry and evolution of the Late Eocene Saveh magmatic complex, central Iran: partial melts of sub-continental lithospheric mantle and magmatic differentiation. Lithos 314–315:274–292

Omrani H (2018) Island-arc and active continental margin adakites from the Sabzevar zone. Iran, Petrology 26:96–113

Omrani J, Agard P, Witechurch H, Benoit M, Prouteau G, Jolivet L (2008) Arc magmatism and subduction history beneath the Zagros Mountains, Iran: a new report of adakites and geodynamic consequences. Lithos 106:380–398

Omrani H, Moazzen M, Oberhansli R (2018) Geodynamic evolution of the Sabzevar Zone, north of the Central Iranian Microcontinent. Mineral Petrol 112:65–83

Pang KN, Chung SL, Zarrinkoub MH, Khatib MM, Mohammadi SS, Chiu HY, Chu CH, Lee HY, Lo CH (2013) Eocene–Oligocene post-collisional magmatism in the Lut–Sistan region, eastern Iran: magma genesis and tectonic implications. Lithos 180:234–251

Pearce J (2008) Gechemical fingerprinting of oceanic basalts with applications to ophiolite classification and the search for Archean oceanic crust. Lithos 100:14–48

Pearce JA, Harris NW, Tindle AG (1984) Trace element discrimination diagrams for the tectonic interpretation of granitic rocks. J Petrol 25: 956–983

Peccerillo AB, Taylor SR (1976) Geochemistry of Eocene calc-alkaline volcanic rocks from the Kastamonu area, Northern Turkey. Contrib Mineral Petrol 58:63–81

Rahmani F, Noghreyan M, Mackizadeh MA (2017) Mineral chemistry of the ultramafic and mafic cumulates in the eastern part of the Sabzevar ophiolite (NE Iran): evidence for formation of high pressure cumulates in thickened arc crust. Neues Jahrb Geol P-A 286(3): 303–328

Rahmani F, Mackizadeh MA, Noghreyan M, Marchesi C, Garrido CJ (2020) Petrology and geochemistry of mafic and ultramafic cumulate rocks from the eastern part of the Sabzevar ophiolite (NE Iran): implications for their petrogenesis and tectonic setting. Geosci Front. https://doi.org/10.1016/j.gsf.2020.02.004

Ramezani J, Tucker RD (2003) The Saghand region, Central Iran: U-Pb geochronology, petrogenesis and implication for Gondwana tectonics. Am J Sci 303(7):622–665

Ranin A, Sepahi AA, Moinvaziri H, Aliani F (2010) Petrology and geochemistry of the plutonic complexes of the Marivan area, Sanandaj-Sirjan zone. Iranian Journal of Petrology 2:43–60

Rossetti F, Nasrabady M, Vignaroli G, Theye T, Gerdes A, Razavi SMH, Moin Vaziri H (2010) Early Cretaceous migmatitic mafi c granulites from the Sabzevar range (NE Iran): Implications for the closure of the Mesozoic peri-Tethyan oceans in central Iran. Terra Nova 22: 26–34

Rossetti F, Nasrabady M, Theye T, Gerdes A, Monié LF, Vignaroli G (2014) Adakite differentiation and emplacement in a subduction channel: The late Paleocene Sabzevar magmatism (NE Iran). GSA Bull 126:317–343

Saccani E, Delavari M, Beccaluva L, Amini S (2010) Petrological and geochemical constraints on the origin of the Nehbandan ophiolitic complex (eastern Iran): Implication for the evolution of the Sistan Ocean. Lithos 117:209–228

Sengör AMC (1990) A new model for the late Paleozoic–Mesozoic tectonic evolution of Iran and implications for Oman. In: Robertson AHF, Searle MP, Ries AC (eds) The Geology and Tectonics of the Oman Region, Geol. Soc. Spec. Publ., vol 49, pp 797–831

Sengör AMC, Altiner D, Cin A, Ustaomer T, Hsu KJ (1988) Origin and assembly of the Tethyside orogenic collage at the expense of Gondwana Land. Geol Soc Spec Publ 37:119–181

Shafaii Moghadam H, Corfu F, Chiaradia M, Stern RJ, Ghorbani G, Rossetti F (2014) Sabzevar ophiolite, NE Iran: progress from embryonic oceanic lithosphere into magmatic arc constrained by new isotopic and geochemical data. Lithos 210–211:224–241

Shafaii Moghadam H, Li XH, Ling XX, Santos JF, Stern RJ, Li QL, Ghorbani G (2015) Eocene Kashmar granitoids (NE Iran): petrogenetic constraints from U–Pb zircon geochronology and isotope geochemistry. Lithos 216–217:118–135

Shafaii Moghadam H, Li XH, Santos JF, Stern RJ, Griffin W, Ghorbani G, Sarebani N (2017) Neoproterozoic magmatic flare-up along the N. margin of Gondwana: The Taknar complex, NE Iran. Earth Planet. Sci Lett 474:83–96

Shafaii Moghadam H, Stern RJ, Griffin WL, Khedr MZ, Kirchenbaur M, Ottley CJ, Whattam S, Kimura JI, Ghorbani G, Gain S, O'Reilly SY, Tamura A (2019) Subduction initiation and back-arc opening north of Neo-Tethys: Evidence from the Late Cretaceous Torbat-e-Heydarieh ophiolite of NE Iran. Geol Soc Am Bull 132(5–6): 1083–1105

Shafaii Moghadama H, Rossetti F, Lucci F, Chiaradia M, Gerdes A, Lopez Martinez M, Ghorbani G, Nasrabady M (2016) The calc-alkaline and adakitic volcanism of the Sabzevar structural zone (NE Iran): Implications for the Eocene magmatic flare-up in Central Iran. Lithos 248–251:517–535

Shen P, Pan HD (2013) Country-rock contamination of magmas associated with the Baogutu porphyry Cu deposit, Xinjiang, China. Lithos 177:451–469

Shojaat B, Hassanipak AA, Mobasher K, Ghazi AM (2003) Petrology, geochemistry and tectonics of the Sabzevar ophiolite, North Central Iran. J Asian Earth Sci 21:1053–1067

Spies O, Lensch G, Mihem A (1983) Geochemistry of the postophiolitic Tertiary volcanics between Sabzevar and Quchan (NE Iran). Report of Geological Survey and Mineral Exploration of Iran 51:247–266

Stampfli GM, Borel GD (2002) A plate tectonic model for the Paleozoic and Mesozoic constrained by dynamic plate boundaries and restored synthetic oceanic isochrones. Earth Planet Sci Lett 196:17–33

Stöcklin J (1974) Possible ancient continental margins in Iran. In: Burk CA, Drake CL (eds) The geology of continental margins. Springer, New York, pp 837–887

Sun SS, McDonough WF (1989) Chemical and isotopic systematics of oceanic basalts: implications for mantle composition and processes. In: Saunders, A. D, Norry, M. J. (eds) Magmatism in the Ocean Basins. Geol. Soc. Spec. Publ. 42: 313–345

Tadayon M, Rossetti F, Zattin M, Nozaem R, Calzolari G, Madanipour S, Salvini F (2017) The post-Eocene evolution of the Doruneh Fault region (Central Iran): The intraplate response to the re-organisation of the Arabia-Eurasia collision zone. Tectonics 36:3038–3064

Tadayon M, Rossetti F, Zattin M, Calzolari G, Nozaem R, Salvini F, Faccenna C, Khodabakhshi P (2018) The long-term evolution of the Doruneh Fault region (Central Iran): A key to understanding the spatio-temporal tectonic evolution in the hinterland of the Zagros convergence zone Geological Journal, 1–26

Taheri J, Shamanian Gh (2001) Geological map 1: 100,000 of Kashmar. Prepared by Geological Survey of Iran

Takin M (1972) Iranian geology and continental drift in the Middle East. Nature 235:147–150

Verdel C, Wernicke BP, Hassanzadeh J, Guest B (2011) A Paleogene extensional arc flare-up in Iran. Tectonics 30

Whitney DL, Evans BW (2010) Abbreviations for names of rock–Forming minerals. Am Mineral 95:185–187

Xiang W, Griffin W, Jie C, Pinyun H, Xiang L (2011) U and Th contents and Th/U ratios of zircon in felsic and mafic magmatic rocks, Improved zircon-melt distribution coefficients. Acta Geol Sin-Engl 85:164–174

Yakymchuk C, Kirkland C L, Clark C (2018) Th/U ratios in metamorphic zircon. J Metamorph Geol 36: 715–737